Bull. Soc. géol. Fr.
BSGF - Earth Sciences Bulletin 2017, 188, 34
© N. Krim *et al.*, Published by EDP Sciences 2017
DOI: 10.1051/bsgf/2017196

BSGF
Earth Sciences Bulletin
Available online at:
www.bsgf.fr

Paleoenvironmental evolution of the southern Neuquèn basin (Argentina) during the Tithonian-Berriasian (Vaca Muerta and Picún Leufú Formations): a multi-proxy approach

Nesma Krim[1,2,*], Cédric Bonnel[2], Nicolas Tribovillard[3], Patrice Imbert[1], Charles Aubourg[2], Armelle Riboulleau[3], Viviane Bout-Roumazeilles[3], Guilhem Hoareau[2] and Bertrand Fasentieux[2]

[1] CSTJF, TOTAL S.A., avenue Larribau, 64018 Pau Cedex, France
[2] Université de Pau et des Pays de l'Adour, Laboratoire des Fluides Complexes et de leurs Réservoirs, UMR CNRS TOTAL 5150, Bâtiment IPRA, BP 1115, 64013 Pau Cedex, France
[3] Université de Lille 1, Laboratoire LOG, UMR CNRS 8187, Bâtiment SN5, 59655 Villeneuve d'Ascq Cedex, France

Abstract – The Tithonian-Berriasian interval in the southern part of the Neuquén Basin is represented by the Vaca Muerta and the Picún Leufú Formations. Facies analysis and correlation of the Vaca Muerta Formation and the lower part of the Picún Leufú Formation in the Picún Leufú Anticline allow us to characterize the evolution of successive facies belts representing siliciclastic shelf and mixed ramp environments. Shoreface and offshore facies are developed on the siliciclastic shelf in the western and southern parts of the Picún Leufú Anticline. The offshore transition domain is characterized by storm beds and slump features, whereas the offshore domain corresponds to black to grey shales and turbidites. The mixed siliciclastic-carbonate ramp is characterized by the development of a lagoon and high-energy shoal in the proximal part of the inner ramp, whereas the distal part comprises a tidal complex. The mid-ramp zone is characterized by storm influence and the outer ramp by fine-grained deposits. Two major transgressive-regressive sequences and five high-frequency transgressive-regressive sequences are recognized. The high-frequency transgressive-regressive sequences make up three progradational sequences, an aggradational-progradational sequence and an aggradational sequence. The geochemical characteristics and clay mineralogy of the Tithonian-Berriasian interval in the southern Neuquén Basin indicate that (1) climate played a key role in the evolution of the sedimentary environment, (2) a "normal marine" depositional environment with oxic sea water and sediment pore waters, rapidly changing to suboxic conditions at shallow depth below the seabed and (3) the occurrence of episodically restricted water-mass circulation at the onset of deposition of the Vaca Muerta Formation.

Keywords: Vaca Muerta Formation / source rocks / siliciclastic shelf / mixed siliciclastic-carbonate ramp / sequence stratigraphy / oxygenation status

Résumé – Évolution paléoenvironnementale de la partie sud du bassin de Neuquèn (Argentine) pendant l'intervalle tithonien-berriasien (formations Vaca Muerta et Picún Leufú) : approche *multi-proxy*. L'intervalle tithonien-berriasien de la partie méridionale du bassin Neuquén est représenté par les formations de la Vaca Muerta et de Picún Leufú. L'analyse de faciès et la corrélation de logs sédimentaires de la formation de la Vaca Muerta et de la partie inférieure de la formation de Picún Leufú dans l'anticlinal Picún Leufú a permis de mettre en évidence un environnement de rampe silicoclastique évoluant vers un environnement de rampe mixte. En environnement de rampe silicoclastique, les faciès de *shoreface* et d'*offshore* se localisent dans les parties ouest et sud de l'anticlinal Picún Leufú. La zone de transition est caractérisée par des niveaux de tempête et des niveaux déstructurés et slumpés, alors que le domaine d'*offshore* correspond à des marnes noires à grises ainsi qu'à des niveaux de turbidites. La rampe mixte silicoclastique-carbonatée se caractérise dans sa partie proximale par le développement d'un lagon isolé du milieu marin ouvert où se déposent des faciès sédimentaires de haute énergie soumis à l'influence de la marée alors que la zone distale est caractérisée par des faciès tidaux. La rampe médiane est caractérisée par

*Corresponding author: nesma.krim@gmail.fr

l'influence des dépôts de tempêtes et la rampe externe par des dépôts à granulométrie fine. Deux séquences transgressives-régressives majeures et cinq séquences transgressives-régressives de haute fréquence sont reconnues. Les séquences transgressives-régressives de haute fréquence forment trois séquences progradantes, une séquence mixte caractérisée par de l'aggradation et de la progradation et une séquence purement aggradante. La caractérisation géochimique et la minéralogie des argiles de l'intervalle tithonien-berriasien dans la partie méridionale du bassin de Neuquén indiquent (1) que le climat a joué un rôle clé dans l'évolution de l'environnement sédimentaire, (2) que l'environnement de dépôt initialement « normal » évolue rapidement vers des conditions suboxiques à l'interface eau-sédiment et (3) la présence d'épisodes où l'oxygénation de la masse d'eau peut être faible principalement au début du dépôt de la formation Vaca Muerta.

Mots clés : formation Vaca Muerta / roches mères / plateforme silicoclastique / rampe carbonatée / stratigraphie séquentielle / degré d'oxygénation

1 Introduction

The Vaca Muerta Formation, deposited during the Late Jurassic-Early Cretaceous, is one of the most petroleum source rocks of the Neuquén Basin (Argentina) (Giusiano *et al.*, 2011). In the context of increasing unconventional oil and gas exploration, the understanding of the paleoenvironmental conditions for the deposit and preservation of these organic-rich rocks is fundamental. Kietzmann and Palma (2011) recognized the presence of precessional and eccentricity orbital cycles in the Tithonian of the northern part of the Neuquén basin, indicating an important climatic control on sedimentation.

This formation consists of dark-brown to black organic-rich shales and mudstones/siltstones, commonly interpreted as deposited under euxinic conditions during a major transgression onto a shelf and slope during the Tithonian to early Valanginian (Legarreta and Uliana, 1991, 1996). Mitchum and Uliana (1985) proposed to subdivide the lower Tithonian-early Valanginian interval of the Vaca Muerta Formation into 10 depositional sequences using seismic stratigraphy and related them to the eustatic sea-level curve.

Kietzmann *et al.*, 2014a, b, c, 2015) recently studied the Vaca Muerta Formation in the northern part of the basin (southern Mendoza and northern Neuquén areas) and identified two orders of transgressive–regressive cycles: five composite depositional sequences and fifteen high-frequency depositional sequences. The whole system shows a regressive trend.

In the southern part of the Neuquén Basin, the Vaca Muerta Formation crops out in the Picún Leufú Anticline. Spalletti *et al.* (2000) studied the sequence stratigraphy of the Tithonian-Berriasian interval in this area and concluded that the Vaca Muerta Formation was deposited on a gentle ramp profile in a restricted gulf-like paleogeography in relation with the uplift of Huincul Ridge (Freije *et al.*, 2002; Zavala *et al.*, 2005). This configuration favoured the development of tide-dominated systems. More recent studies in the southern part of the basin (Zeller, 2013; Massaferro *et al.*, 2014; Zeller *et al.*, 2014) led to the identification of three Major Sequences in the Picún Leufú Anticline with the high input of siliciclastic material explained by an along-shelf current mechanism. Using seismic data, these authors established a direct connection between the southern part of the basin (Picún Leufú depocentre) and the Neuquén Embayment.

The aim of this study is to provide a paleoenvironmental model for the southern part of the Neuquén Basin and document its evolution, in order to enrich and update our understanding of silt-rich hydrocarbon source rocks. This study focuses on the lower part of the Vaca Muerta Formation and therefore supplements the studies of Massaferro *et al.* (2014), Zeller (2013) and Zeller *et al.* (2014) concerning the upper part of the Vaca Muerta Formation and the Picún Leufú Formation in this part of the basin, as well as the work of Kietzmann *et al.* (2014a, b) tto the north of the Huincul Ridge. We provide an integrated sedimentary and geochemical characterization of the lower part of the Vaca Muerta Formation in the Picún Leufú Anticline, located in the southern part of the Neuquén Basin. The Picún Leufú Anticline shows high-quality outcrops in the studied interval. The sedimentological description of twelve sections is supplemented with mineralogical and geochemical analyses on one section.

2 Geological setting and stratigraphy

The Neuquén Basin (Fig. 1) of western Argentina and eastern Chile is located between latitudes 32° S and 41° S and covers an area of over 120 000 km^2 (Yrigoyen, 1991). It has a triangular shape and is bounded by the Sierra Pintada Massif to the northeast, the Patagonian Massif to the south and the Andean Arc to the west (Legarreta and Gulisano, 1989; Howell *et al.*, 2005).

Two main sectors are recognized in the Neuquén Basin: the Neuquén Andes to the west, where Late Cretaceous-Cenozoic deformation has led to the development of fold and thrust belts, and the Neuquén Embayment to the east and south-east where most of the Mesozoic sedimentary succession is relatively undeformed (Legarreta and Gulisano, 1989; Legarreta and Uliana, 1991, 1996).

The evolution of the Neuquén Basin can be considered as consisting of three stages (Legarreta and Gulisano, 1989; Legarreta and Uliana, 1991, 1996; Howell *et al.*, 2005):

- from the Late Triassic to Early Jurassic (rifting stage): this part of Gondwana was characterized by extensional tectonics and the development of a series of narrow and isolated half-grabens, filled with continental and volcanic red-bed facies (Manceda and Figueroa, 1995; Vergani *et al.*, 1995; Franzese and Spalletti, 2001);
- from the Early Jurassic to Early Cretaceous (post-rift stage): regional thermal subsidence (Legarreta and Gulisano, 1989; Legarreta and Uliana, 1991) related to

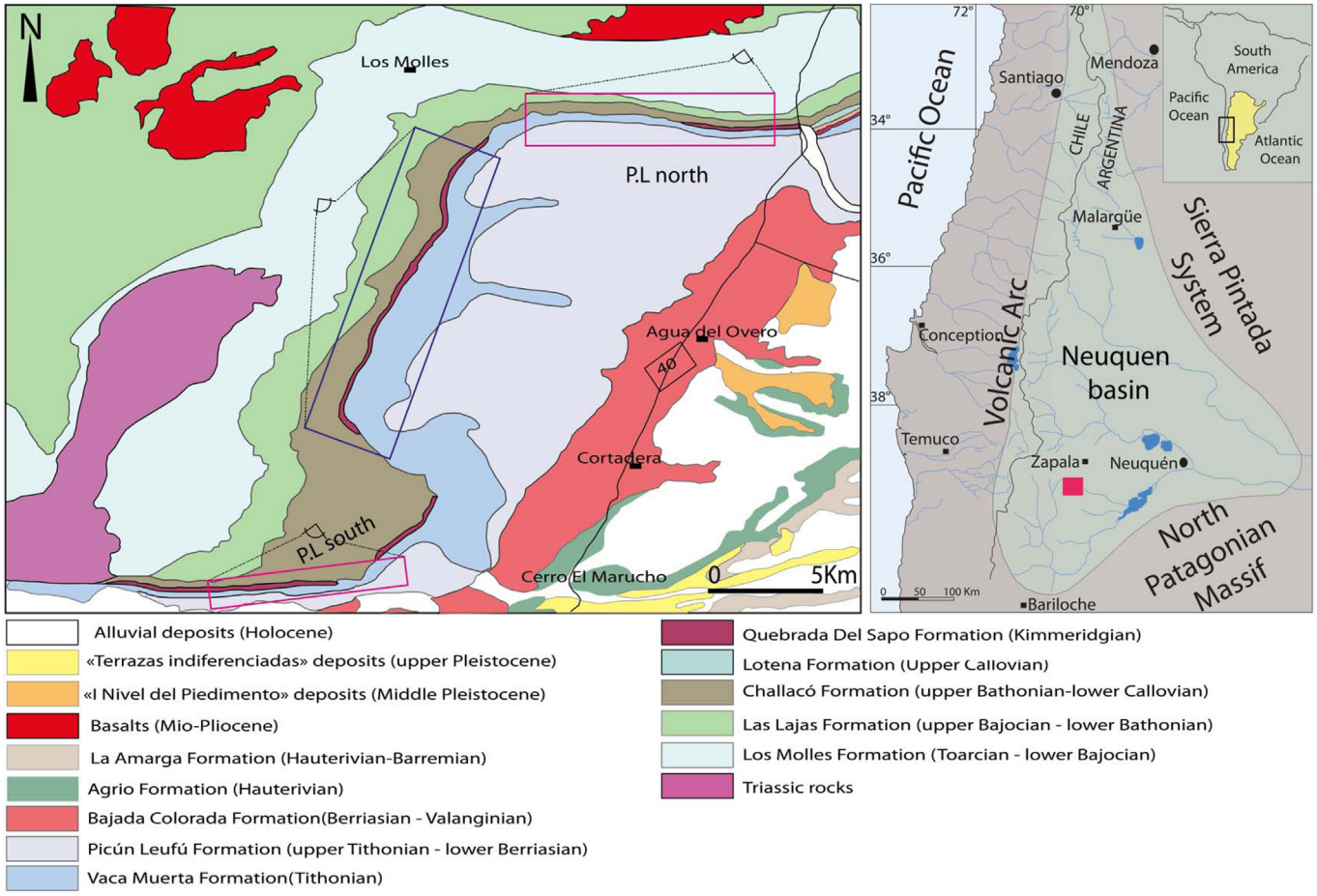

Fig. 1. Location map of the Neuquén Basin and geological map of the Picún Leufú Anticline (red box indicates the location of measured sections, blue box indicates observation reported in the western side of the Picún Leufú Anticline).

subduction along the western margin resulted in the development of a wide marine Embayment and the accumulation of more than 4000 m of marine and continental deposits (Vergani *et al.*, 1995);

– from the Late Cretaceous to Cenozoic: the basin was characterized by a compressional tectonic regime associated with a decrease in the angle of slab subduction that produced the uplift of the foreland thrust belt (Ramos, 1999). Flexural subsidence towards the east of the tectonic front allowed the accumulation of more than 2000 m of continental syn-orogenic deposits (Legarreta and Uliana, 1991; Ramos, 1999).

Thus, from Early Jurassic to Early Cretaceous times, the Neuquén Basin was a retro-arc basin, associated with the subduction of the proto-Pacific crust beneath the western margin of Gondwana (Vergani *et al.*, 1995). The long period of thermal subsidence and regional back-arc extension led to the development of a marine basin that was connected to the proto-Pacific Ocean by gaps in the arc (Spalletti *et al.*, 2000; Macdonald *et al.*, 2003). A complex series of transgressive-regressive cycles developed during this period due to variations in subsidence rate, eustatic sea-level fluctuations and localized uplifts (Fig. 2; Gulisano *et al.*, 1984; Legarreta and Gulisano, 1989; Legarreta and Uliana, 1991, 1996).

The regime of regional thermal subsidence was interrupted by several episodes of structural inversion (Vergani *et al.*, 1995; Veiga *et al.*, 2001; Pángaro *et al.*, 2002) corresponding to the Peruvian (Upper Cretaceous), Incaic (Eocene) and Quechua compressional phase (Miocene to actual). These tectonic inversions caused and/or enhanced relative sea-level falls and resulted in the accumulation of six wedges, sharply overlying deep-marine deposits. These lowstand wedges generally consist of continental deposits and are spatially restricted to the central part of the basin (Legarreta, 2002). In the marginal areas of the basin, the tectonic inversions are often represented by angular unconformities between sedimentary units forming important hiatus surfaces (Veiga and Spalletti, 2007).

In the southern part of the basin, a major tectonic inversion occurred during late Oxfordian to Kimmeridgian times, related to a change in the subduction regime along the active margin of the basin (Vergani *et al.*, 1995). A reconfiguration of the basin at this time was associated with the uplift of the Huincul Ridge, which divided the wide Embayment of the Neuquén Basin into two main sedimentary depocentres (Zavala *et al.*, 2005; Mosquera and Ramos, 2006).

The Huincul Ridge formed a structural high and paleogeographical barrier that isolated the southern depocentre. Thickness analysis of the Tordillo Formation suggests

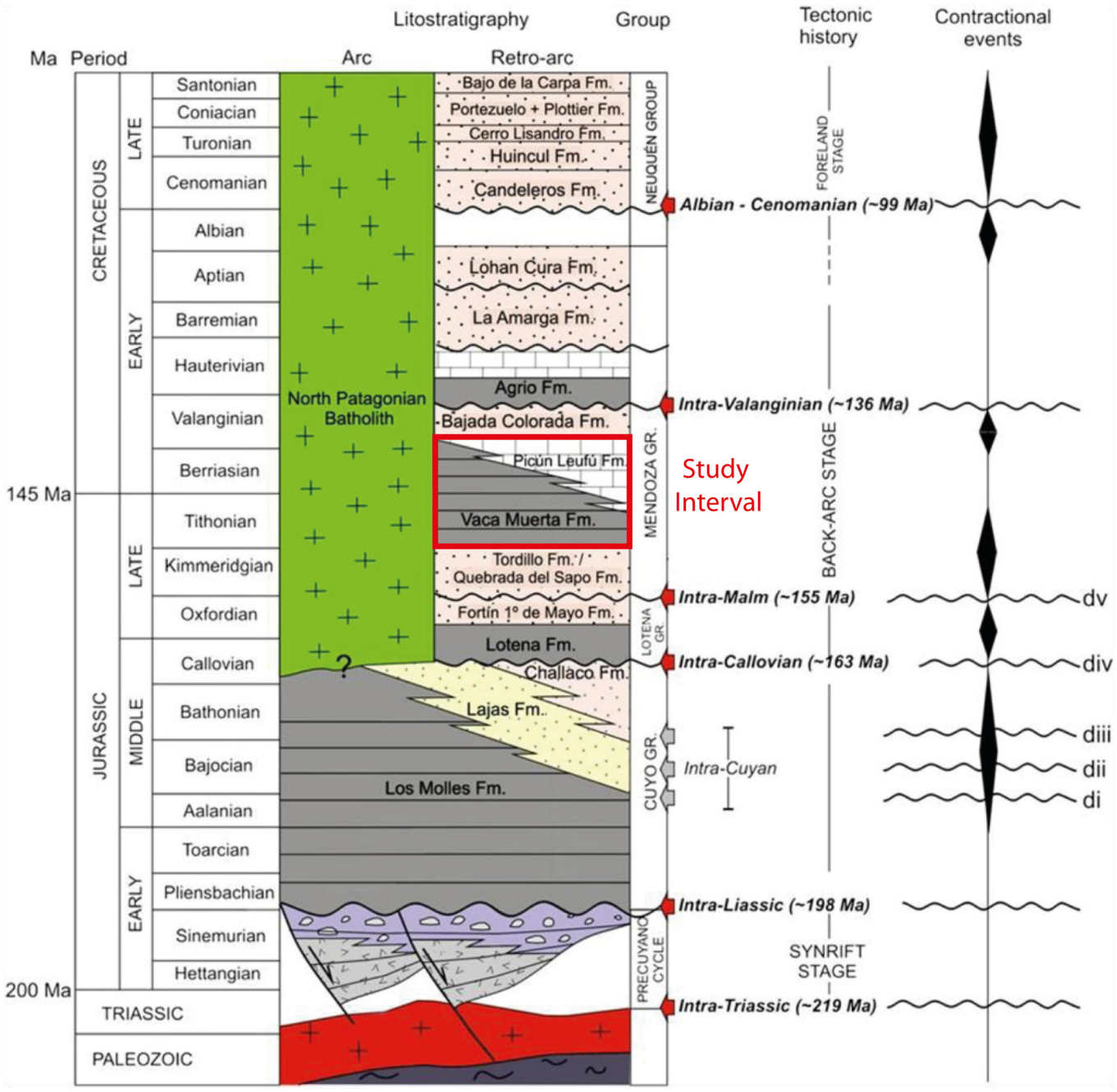

Fig. 2. Tectonostratigraphic chart of the southern Neuquén Basin and adjacent sectors, showing main unconformities and timing of deformation (Naipauer *et al.*, 2012).

the existence of two depocentres in the northern part of the basin (Vergani *et al.*, 1995; Spalletti and Colombo Piñol, 2005). In the southern part of the basin, the Kimmeridgian sediments correspond to < 40 m-thick fluvial deposits of the Tordillo Formation (Groeber, 1946) grading into the eolian deposits of the Quebrada Del Sapo Formation (Digregorio, 1972). This observation suggests a structural activity of the Huincul Ridge before the Tithonian, whereas a recent study (Massaferro *et al.*, 2014) suggests that the tectonic activity of the Huincul Ridge was initiated during the Late Berriasian with a maximum height during the Early Valanginian (Freije *et al.*, 2002).

The Tithonian-Berriasian interval is the object of the present study (Fig. 3). In most of the Neuquén Basin, the uppermost Jurassic-lowermost Cretaceous deposits corresponds to the dark bituminous shales, marls and carbonates of the Vaca Muerta Formation (Weaver, 1931; Leanza, 1973) and its lateral shallow water facies equivalent. The contact between the underlying Tordillo Formation (Groeber, 1946) and the Vaca Muerta Formation is erosive (Freije *et al.*, 2002), considered to be isochronous and marks the beginning of the marine Tithonian transgression (Leanza, 1981). This coincides with an episode of regional subsidence attributed to post-compressional relaxation (Vergani *et al.*, 1995). The top of the

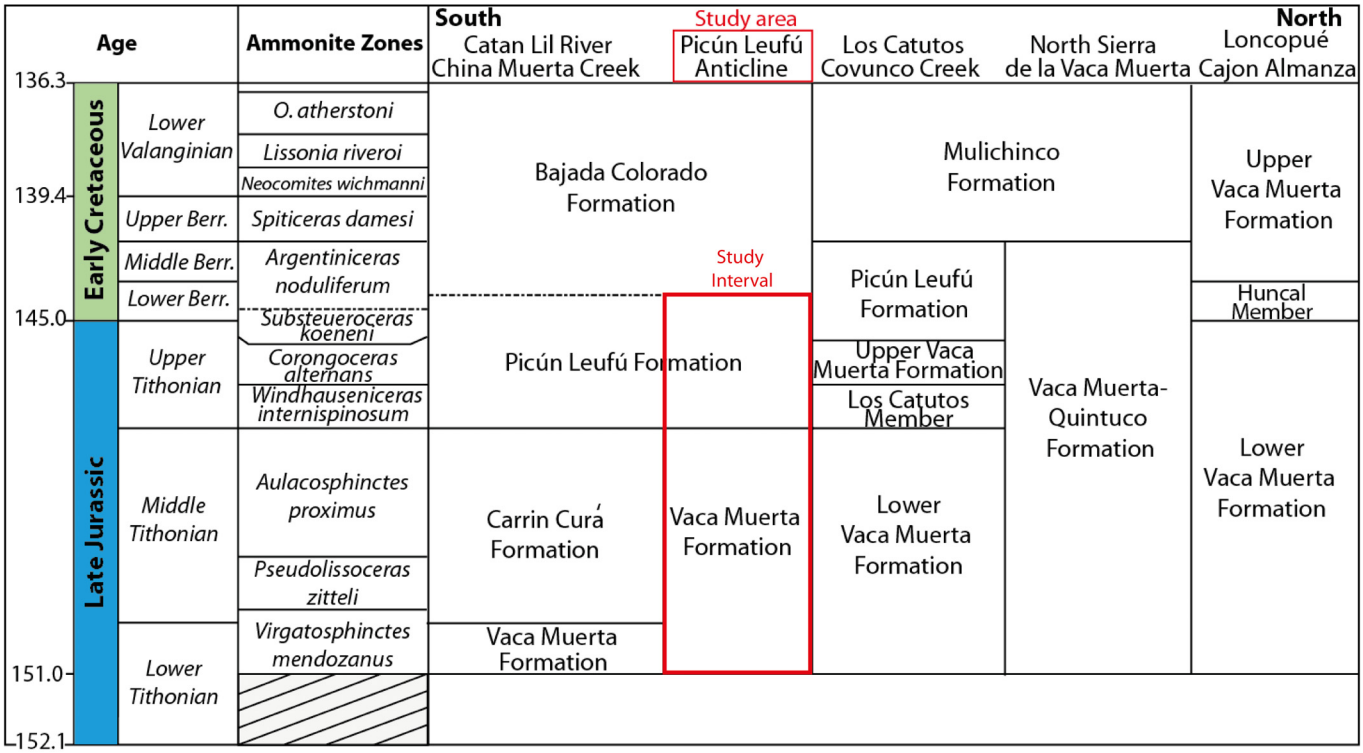

Fig. 3. Chronostratigraphic chart of the Tithonian– early Valanginian in the southern and central Neuquén Basin (Modified after Spalletti *et al.*, 2000). Huncal Member from Leanza *et al.* (2003). Time scale after Gradstein *et al.* (2012). Ammonite biozones from Leanza and Zeiss (1994), Riccardi (2008), Aguirre-Urreta *et al.* (2011).

Vaca Muerta Formation is diachronous (Leanza, 1973, 1981, 1994; Leanza and Hugo, 1978; Leanza *et al.*, 1978) and progradational becoming younger toward the central area of the basin (Gulisano *et al.*, 1984; Mitchum and Uliana, 1985; Legarreta and Gulisano, 1989) (Fig. 3).

In the southern part of the basin, the Tithonian–Berriasian interval comprises two marine lithostratigraphic units known as the Vaca Muerta and Picún Leufú Formations (Leanza, 1973). The Vaca Muerta Formation (locally dated as Lower to earliest lowermost Upper Tithonian) consists of a thick succession of dark bituminous shales and marls, whereas the Picún Leufú Formation consists of mixed carbonate and siliciclastic sediments (Armella *et al.*, 2007; Spalletti *et al.*, 2000). In this part of the basin, Spalletti *et al.* (2000) interpreted the Tithonian-lower Berriasian succession (Vaca Muerta-Picún Leufú Formations) as being deposited on a gently sloping marine ramp (mixed siliciclastic-carbonate deposits) with a gradual transition from a shallow marine area along the southern and southwestern margins of the basin towards deeper areas in the north.

In the central part of the basin (Neuquén Embayment), the Vaca Muerta Formation consists of basinal deposits, which grade eastward into the shoreface deposits of the Quintuco Formation (upper Tithonian–lower Valanginian) and the sabkha deposits of the Loma Montosa Formation (lower Valanginian), forming a mixed carbonate-siliciclastic depositional system (Mitchum and Uliana, 1985; Gulisano *et al.*, 1984; Carozzi *et al.*, 1993). To the west, the Vaca Muerta Formation includes slope facies (the Huncal Member), and, in Chilean territory, passes into shallow marine/volcanic deposits (Charrier, 1985; Leanza *et al.*, 2011; Kietzmann and Vennari, 2013).

In the north of the basin (southern Mendoza area), Kietzmann *et al.* (2014a) also interpreted the Vaca Muerta deposits as the westward progradation of a homoclinal carbonate ramp located on the eastern margin of the basin, whereas the western margin represents the outer part of a distally steepened ramp prograding eastward.

The major difference between the north and the south is related to variations in siliciclastic input due to differences in latitudinal position (Volkheimer *et al.*, 2008) as well as tectonic reactivation of the Huincul Ridge (E-W structure) and the Chihuidos High (large structure developed parallel to the Andean Arc) (Vergani *et al.*, 1995; Maretto and Pangaro, 2005).

3 Materials and methods

The study area is located in the southern part of the Neuquén Basin. This area is located in the Picún Leufú Anticline (Fig. 1), close to the town of Zapala, extending between latitude 39°16’ and 39°25’ S and between longitude 69°58’ and 70°19’ W.

The east-west oriented Picún Leufú Anticline defines the western portion of the Huincul Ridge and forms the main topographic feature of the region (Marchese, 1971). In the Picún Leufú zone, the Tithonian–Berriasian interval

corresponds to two marine lithostratigraphic units known as the Vaca Muerta and Picún Leufú Formations (Leanza, 1973). The Vaca Muerta– Picún Leufú interval was studied at several points of the Picún Leufú Anticline. Eight sections numbered log #1 to log #8 were studied on the northern flank of the Picún Leufú Anticline, while four sections numbered log #9 to log #12 were studied on the southern flank. The spacing between the studied sections in each sector varies between 1 and 2 km. Sections were logged at a scale of 1:100 (Fig. 4) using a Jacob's staff to measure bed thicknesses. Texture, sedimentary structures, thickness, geometry and spatial relationships were documented during fieldwork. In addition, satellite images and photographs were used to investigate the western flank of the anticline, corresponding to an Indian territory where we do not have authorization for access.

Only the log #3 was sampled for petrographic and geochemical analyses as well as characterization of clay mineral content. Fifty-nine samples were collected along the 450-m-thick section. Ten samples were taken with an average spacing of 1.5 m in the basal fifteen meters of the studied interval to analyze in detail the black shales, and fourty-nine samples were taken along the section, but without a regular spacing, to obtain the overall evolution of the studied interval.

Rock-Eval pyrolysis (Espitalié *et al.*, 1977, 1985) was made, using a Rock Eval 6 (VINCI Technologies, [Behar *et al.*, 2001]) at Total (Pau, France). The carbonate content was determined with a Bernard-type calcimeter (acid digestion followed by CO_2 volume determination; accuracy $< 5\%$). The clay fraction was isolated and analyzed using the standard protocol for determining clay-mineral assemblages (using a Bruker D4 Endeavour XRD system together with the Macdiff software; see detailed protocol in Bout-Roumazeilles *et al.*, 1999). The major- and trace-element contents were analyzed by ICP-OES (Thermo Fischer ICap 6500) and ICP-MS (Thermo Elemental X7) at the SARM-CRPG-CNRS facility in Vandoeuvre-les-Nancy. (geochemistry laboratory of the French Centre National de la Recherche Scientifique). The samples were prepared by fusion with $LiBO_2$ followed by HNO_3 dissolution. Precision and accuracy were both better than 1% (mean 0.5%) for major-minor elements and 5% for trace elements, as checked by international standards and analysis of replicate samples (See standard list using http://helium.crpg.cnrs-nancy.fr/SARM/pages/geostandards.html) (Carignan *et al.*, 2001). Enrichment factors (EF) were calculated as: $XEF = [(X/Al)_{sample}/(X/Al)_{PAAS}]$, where X and Al represent the weight % concentrations of element X and Al, respectively (*e.g.*, Brumsack, 2006; Tribovillard *et al.*, 2006). Samples were normalized using the post-Archean average shale (PAAS) compositions of Taylor and McLennan (1985). Aluminum normalization is commonly used to minimize the effects of variable dilution by carbonate or biogenic silica, although certain caveats apply to this approach (for a discussion, see Van Der Weijden, 2002; Tribovillard *et al.*, 2006; Bomou *et al.*, 2013). Al-normalizations cannot be applied when:

- the coefficient of variation values (standard deviation divided by the mean) of Al content is large relative to the coefficients of the other variables, which may be the case when the detrital fraction is lower than 3–5%;
- Al contents are in marked excess compared to other terrigenic elements.

In our case, the Al-normalization may be applied. The convenience of using enrichment factors is that any normalized value greater than 1.0 corresponds to enrichment of an element relative to its average crustal abundance.

The interpretations of the abundances of redox-sensitive trace and/or productivity-proxies are based on recently published general considerations (Brumsack, 2006; Tribovillard *et al.*, 2006; Algeo and Rowe, 2012; and references therein).

4 Facies analysis

4.1 Facies association type

The present study is mainly grounding on facies analysis on the twelve measured sections. Log sections were measured in the north and the south flanks of the Picún Leufú Anticline (Fig. 1). Twenty-three sedimentary facies are defined on the basis of textural properties and sedimentary structures, and are summarized in Table 1.

4.1.1 Facies association 1 (F.A. 1)

Description: This facies association occurs in the lower half of all measured sections (Fig. 5A and B). It consists of massive and/or laminated black to grey shales (F1) interbedded with rare siltstones (F4) to fine-grained sandstones (F5) (Fig. 5C). The black shale facies (Fig. 5D) consists of massive (F1.a) to laminated (F1.b) black shales to silty shales and occurs only in the basal few meters of the measured section. Grey shales (Fig. 5F) correspond also to massive (F2.a) to laminated (F2.b) silty shales, the latter with mm-thick brown laminae. Fish scales and very scarce ammonites are generally observed, except at the bottom of each measured section where an important ammonite-rich horizon (Fig. 5E) is developed. The interbedded sandstones are massive and tabular, displaying sharp bases and tops. These interbeds are thin and reach a thickness of no more than a few decimeters.

Shaly intervals show an average TOC content of 2%, with maximum values reaching 24% on the first sample at the base of the section. This sample corresponds to laminated shales. This facies association contains several levels of sub-spherical concretions that can be massive or show septarian cracks. They can reach 50 centimeters in diameter and occur in sandy and shaly intervals.

XRD analyses of the grey silty shales show a clay mineralogy essentially composed of smectite (61%) and kaolinite (33%).

Interpretation: The dark color, fine-grained composition and laminated structure of the shales indicate deposition by settling out from suspension in a low-energy environment, probably below the storm wave base. The preservation of lamination, the presence of fish scales and the high organic content suggest an anoxic to sub-oxic environment. Sand beds are attributed to gravity flows probably triggered by storm surges (Wallace-Dudley and Leckie, 1993). The occurrence of ammonites with no trace of reworking indicates an open shelf environment. The ammonite-rich horizon level was analyzed in detail by Parent *et al.* (2011). This ammonite horizon is interpreted as a condensed interval resulting from a low sedimentation rate after an erosional event (Freije *et al.*, 2002).

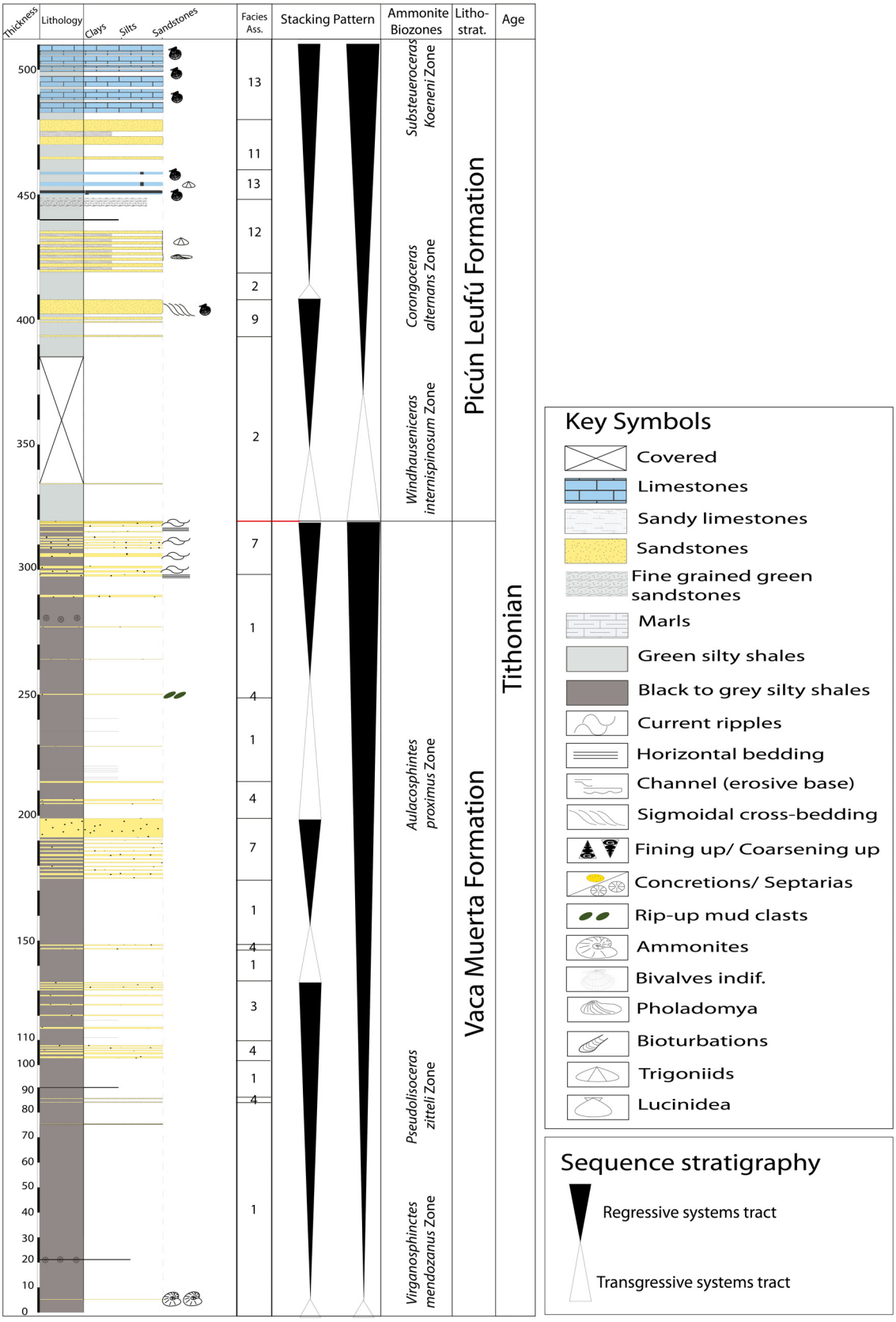

Fig. 4. Log- section (log #7) of the Vaca Muerta Formation in the Picún Leufú Anticline. (Ammonite zones from Leanza, 1973, 1980; Leanza and Zeiss, 1990, 1992; Parent *et al.*, 2011).

Table 1. Sedimentary facies in the studied outcrops.

Facies	Lithology	Sedimentary structures	Bioclastic and other components
1	Black shales to silty shales	Massive (F1.a) to laminated (F1.b)	Ammonites
2	Grey shales to silty shales	Massive (F2.a) to laminated (F2.b)	/
3	Green silty shales	Massive (F3.a) to laminated (F3.b)	Trigoniids
4	Siltstones	/	/
5	Fine-grained sandstones	Massive, some normal grading Planar lamination	Rare mud clasts
6	Sandstones	Massive. Flute casts, crude planar laminations	/
7	Sandstones	Massive	Scarce vertical burrows and bivalve's fragments
8	Sandstones	Massive with internal deformation, scarce planar lamination	/
9	Sandstones	Cross-bedded	Scarce bivalves, bivalve fragments, mud clasts
10	Sandstones	Planar laminations	Scarce bivalves
11	Sandstones	Wave ripples	Scarce bivalves
12	Sandstones	Trough cross-stratification	Scarce bivalves
13	Sandy limestone	Cross-beds	Burrows, mud clasts
14	Sandstones	Sigmoidal cross-bedding, lenticular bedding, wavy bedding, flaser bedding	Scarce bivalve's fragments, mud clasts
15	Green very fine-grained marly sandstones to marls	/	Scarce bivalves and bivalve's fragments
16	Sandy limestone	Trough cross-stratification	Abundant. Bivalves on tops, Trigoniids, and bioturbation
17	Sandstones	Massive	Fragments of trigoniids, *pholadomya*, scarce ammonites/ammonoids and undifferentiated bivalves.
18	Sandy limestones	Massive and channelized, rare planar lamination at the tops.	Bivalve fragments
19	Sandstones	Massive	/
20	Limestones	Mottled, crude lamination	Lucinidea, *Pholadomya*, undetermined bivalves and occasionally scarce oysters
21	Sandstones	Bird's eyes	Abundant bivalves and scarce gastropods
22	Sandy limestones	Bird's eyes	Abundant bivalves and scarce gastropods
23	Amalgamated sandstones	Trough cross-stratification, planar lamination. Rare erosive bases	/

Concretions and septarias are interpreted as being formed in the early diagenetic stages during a decrease or break in sedimentation (Hesse and Schacht, 2011). Facies association 1 is interpreted as representing an offshore zone setting.

4.1.2 Facies association 2 (F.A. 2)

Description: This facies association (Fig. 5A and G) occurs in the upper half of all the measured sections. It consists of massive (F3.a) and/or laminated (F3.b) green silty shales (Fig. 5G and H), interbedded with fine-grained sandstones (F5). Silty green shales contain scarce fossils represented by well-preserved trigoniids. Sand beds are massive, tabular and reach a few centimeters to a few decimeters in thickness with sharp bases and tops.

This facies association displays very low TOC contents (average value $< 0.1\%$). Several levels of concretions are observed both in the sandy and shaly intervals, corresponding to septarian or simple concretions that can reach a diameter of 50 centimeters.

XRD analyses of the green silty shales show differences in clay mineralogy compared to the silty grey shales (F.A. 1). Green silty shales of facies association 2 are richer in smectite (84% *vs.* 61% in F.A. 1) and chlorite (5% *vs.* 0% in F.A. 1), while kaolinite shows an inverse trend (1% *vs.* 33% in F.A. 1).

Interpretation: The fine-grained composition and laminated structure of the green silty shales indicates deposition by settling out of sediment from suspension in a low-energy environment, probably below the storm wave base. The occurrence of sandstone beds suggests a slightly higher energy. As with facies association 1, these beds are attributed to the distal deposition of gravity flows probably triggered by storm surges (Wallace-Dudley and Leckie, 1993). Septarian-type and simple concretions are interpreted as resulting from a low sedimentation rate (Hesse and Schacht, 2011). Facies

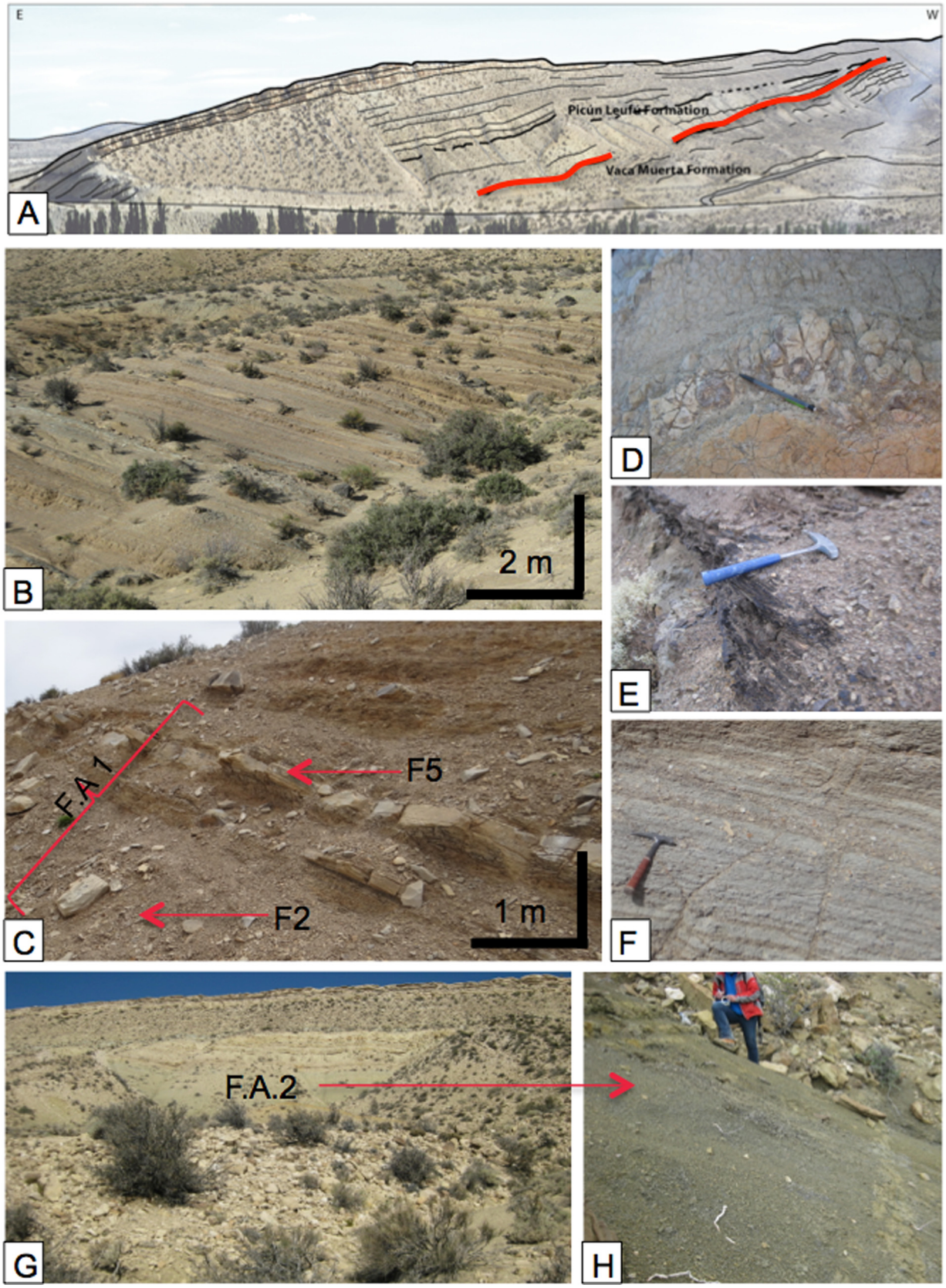

Fig. 5. (A) Outcrop view of studied zone (north Picún Leufú Anticline); (B) General aspect of grey laminated shales (Facies 2); (C) Facies association 1 corresponding to massive and laminated grey shales (F2.a and F2.b, respectively) with rare fine-grained sandstones (Facies 5); (D) Detail of dark shales (Facies 1); (E) Well-preserved ammonoid horizon recognized at the base of the measured sections; (F) Detail of laminated grey shales (Facies 2b); (G) General aspect of green massive shales (Facies 3a); (H) Detail of green massive shales (Facies 3a).

association 2 is interpreted as a distal environment in an offshore transition zone setting.

4.1.3 Facies association 3 (F.A. 3)

Description: This facies association is composed of an alternation of massive sandstones (F6) with minor silty shales (F2), which can reach more than ten meters in thickness. Sandstones vary from a few centimeters to several decimeters in thickness and exhibit sharp bases with flute casts and planar tops (Fig. 6A). They are massive and exhibiting normal grading. Silty shales are grey in colour and can display laminations. Fossils are absent from this facies association.

Interpretation: Massive sandstones can be interpreted as indicating a rapid deceleration and abrupt termination of high-density turbidity currents (Bouma, 1962; Aigner, 1982; Lowe, 1982; Mutti, 1992). Flute marks are interpreted as resulting from an initial phase of high turbulence at the beginning of the flow (Allen, 1982). Laminated silty shales can be considered as the result of settling out of sediment from suspension in a low-energy environment. The alternation between the two facies suggests a combination of (1) turbidity currents and (2) deposition of "mud" from suspension in the water column. Facies association 3 is attributed to turbidite deposits in an offshore setting.

4.1.4 Facies association 4 (F.A. 4)

Description: This facies association is composed of silty shales (F2, Fig. 6B) and massive sandstones (F5, F6). Silty shales are grey-brownish in color, massive and structureless. The sandstone beds are 40 to 50 centimeter thick, characterized by sharp bases and tops (F5) Fig. 6C). Some beds exhibit planar lamination and mud clasts (Fig. 6D). They can also exhibit erosive bases (F6), bivalve fragments and vertical burrows. The sandstone beds do not show any specific trend.

Interpretation: Laminated silty shales can be considered as the result of the deposition of sediment settling out from suspension in a low-energy environment. High velocities planar laminations in some sandstone can be considered as resulting from tractive currents, while structureless sandstones can be interpreted as storm-related deposits, reflecting the waning flow regime of storm-generated currents (Brenchley *et al.*, 1993). The occurrence of mud clasts suggests deposition under turbulent erosion of a mud-rich basin-floor (Zakaria *et al.*, 2013). Facies association 4 was probably deposited in an offshore environment, between the fair weather wave base and the storm wave base. Its deposition reflects episodic, short-lived, high-energy conditions alternating with longer periods of lower energy (fine-grained intervals).

4.1.5 Facies association 5 (F.A. 5)

Description: This facies association is characterized by deformed sandstones (F8) interbedded with grey silty shales (F2). Sandstone beds show scarce planar laminations. They have a thickness of a few decimeters to a few meters and exhibit a folded shape, sometimes with internal deformation (Fig. 7A and B) and lateral pinch-out geometry.

Interpretation: The folded facies and deformed internal layers are considered as evidence for plastic deformation during mass transport. The occurrence of planar lamination in some deformed beds suggests that the material was initially deposited by high-energy tractive currents. This facies association is interpreted as a result of a slumping, probably due to the collapse of a sediment pile through slope instability in the transition zone.

4.1.6 Facies association 6 (F.A. 6)

Description: This facies association consists of sandstones (F9) with fine to very-fine-grained interbeds (F15 and F3). The sandstones are amalgamated or separated by fine-grained interbeds. The sandstone beds are mainly of decimetric to metric in thickness, exhibiting sharp bases and tops and containing mud clasts. Fine to very fine-grained intervals correspond to green shales (F3) that grade laterally into structureless, massive and very fine-grained green sandstones (F15). Some beds contain scarce bivalves and bivalve fragments.

Interpretation: The amalgamation of sandstone beds makes it difficult to recognize the first- and second-order surfaces and internal structures in detail. The presence of mud clasts and bivalve fragments suggests the influence of reworking/remobilization processes. The common occurrence of amalgamated sandstones suggests a lower shoreface environment, but the lateral facies relationship between green shales and very fine green sandstones implies that amalgamation occurred below fair weather wave base. Facies association 6 is interpreted as having been deposited in a mid-ramp setting.

4.1.7 Facies association 7 (F.A. 7)

Description: This facies association consists of sandy beds with various sedimentary structures (F10, F11 and F12) (Fig. 7C–F) and fine-grained intervals (F2). Sandy beds show planar laminations (F10), wave ripples (F11) and scarce ripple cross-stratification (F12). The beds are few decimeters thick to 1 meter, exhibiting sharp bases and tops. Fine-grained interbeds correspond to massive grey silty shales (F2). Rare mud clasts and bivalves can be observed.

Interpretation: The presence of various sedimentary structures reflects deposition by wave and/or current processes. Trough cross-stratifications in sands suggest formation by the migration of sand dunes (longshore currents) in a shallow-water environment. High-energy planar lamination and cross-bedded sandstones are interpreted as deposits of the surf zone. The rare mud clasts can be interpreted as a result of erosional currents. Facies association 7 was deposited above fair weather wave base. It is interpreted to have been deposited on the shoreface.

4.1.8 Facies association 8 (F.A. 8)

Description: This facies association is composed of trough cross-stratification sandy limestones (F13) that reach a few meters in thickness. They are characterized by sharp bases and top and display current ripples and cross-bedding, mud clasts and burrows. The foresets are always directed toward the east on the east-west trending outcrop. These units are interbedded with very-fine-grained green sandstones (F15).

Interpretation: Cross-bedded sandy limestones also suggest a hydrodynamic process driven by unidirectional flow. The occurrence of mud clasts is interpreted as resulting from high flow velocity. Facies association 8 was deposited

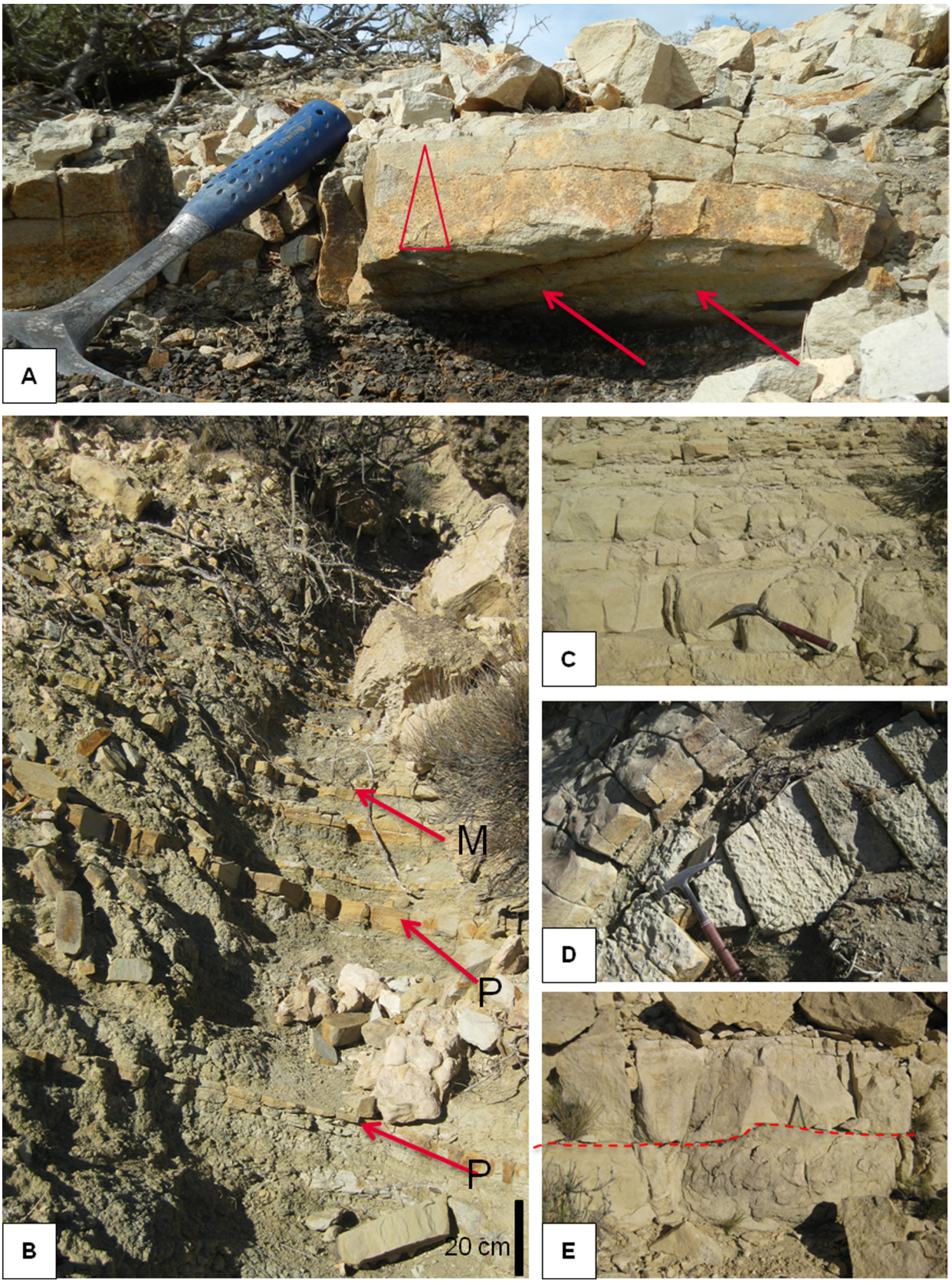

Fig. 6. (A) Turbidites of F.A. 3. (B) to (E) Facies association 4. (B) Alternation of massive (M) or laminated (P) sandstones (F5) and silty shales (F2) of F.A. 4; (C) Sandstones display sharp bases and tops; (D) Some beds contain mud clasts; (E) Sandstone with erosive base (F7) alternating with grey silty shale interbeds (F2).

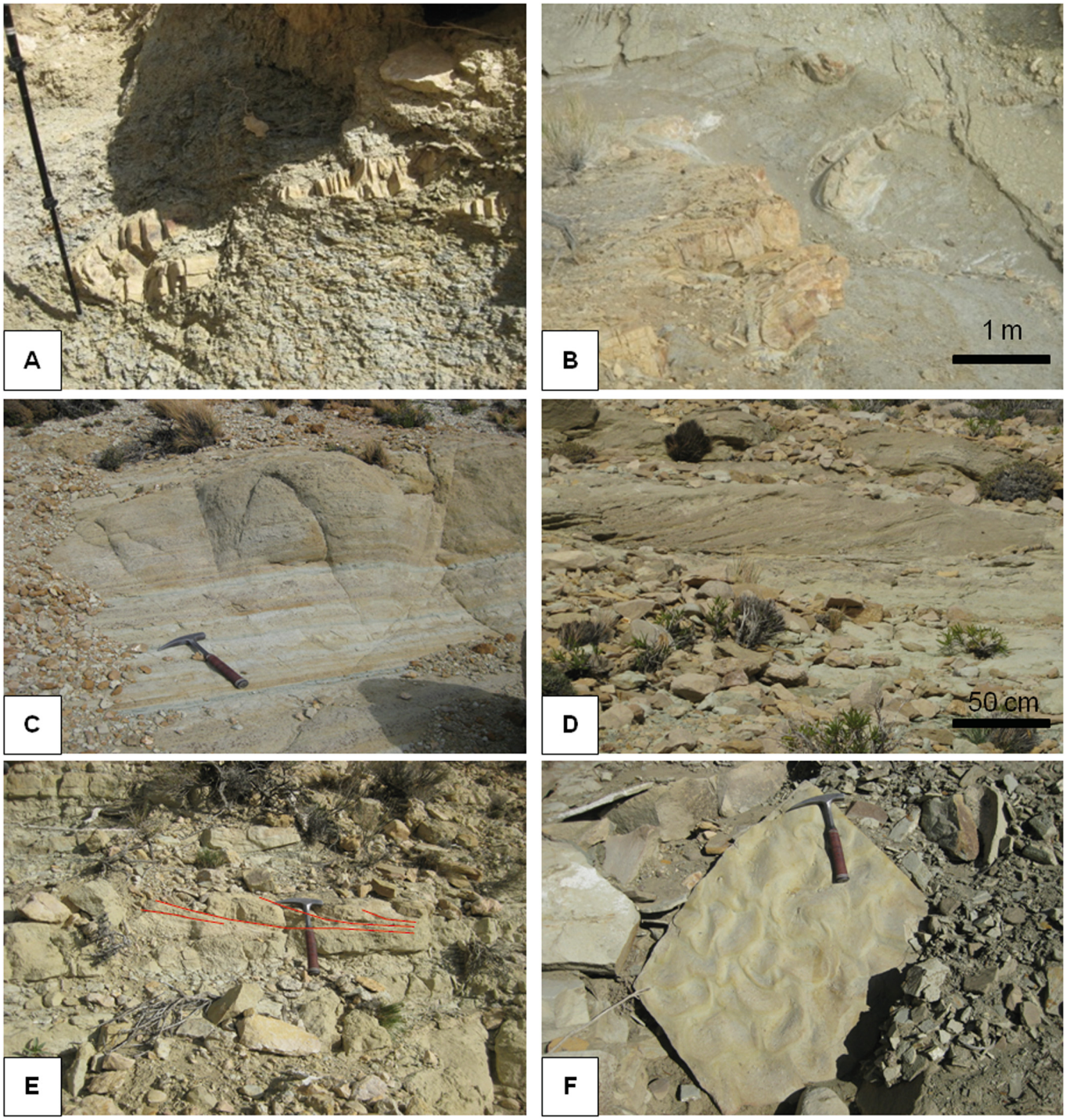

Fig. 7. (A) and (B) illustration of sandstone slumps of F.A. 5; (C) Fine-grained sandstones with planar laminations (F10); (D) Cross-stratified sandstones (F11). (E) and (F) Sand-rich facies with trough cross-bedding (E) and sinuous ripple morphology (F).

probably in a distal inner-ramp to proximal mid-ramp environment.

4.1.9 Facies association 9 (F.A. 9)

Description: This facies association is composed of trough cross-bedded sandstones and minor fine to very-fine-grained green sandy intervals (F15). The sand-rich units (F14) show sharp bases and tops and exhibit large-scale sigmoidal cross-bedding (Fig. 8A). Some units exhibit concave and erosive bases. Sandstones units can reach tens of meters in thickness and show overall fining-upward and thinning. Some units show an upward evolution from lenticular bedding, wavy bedding to flaser bedding (in the sense of Reineck and Wunderlich, 1968) (Fig. 8B). Herringbone cross-stratification can be observed. Mud clasts (Fig. 8C) and mud drapes occur on

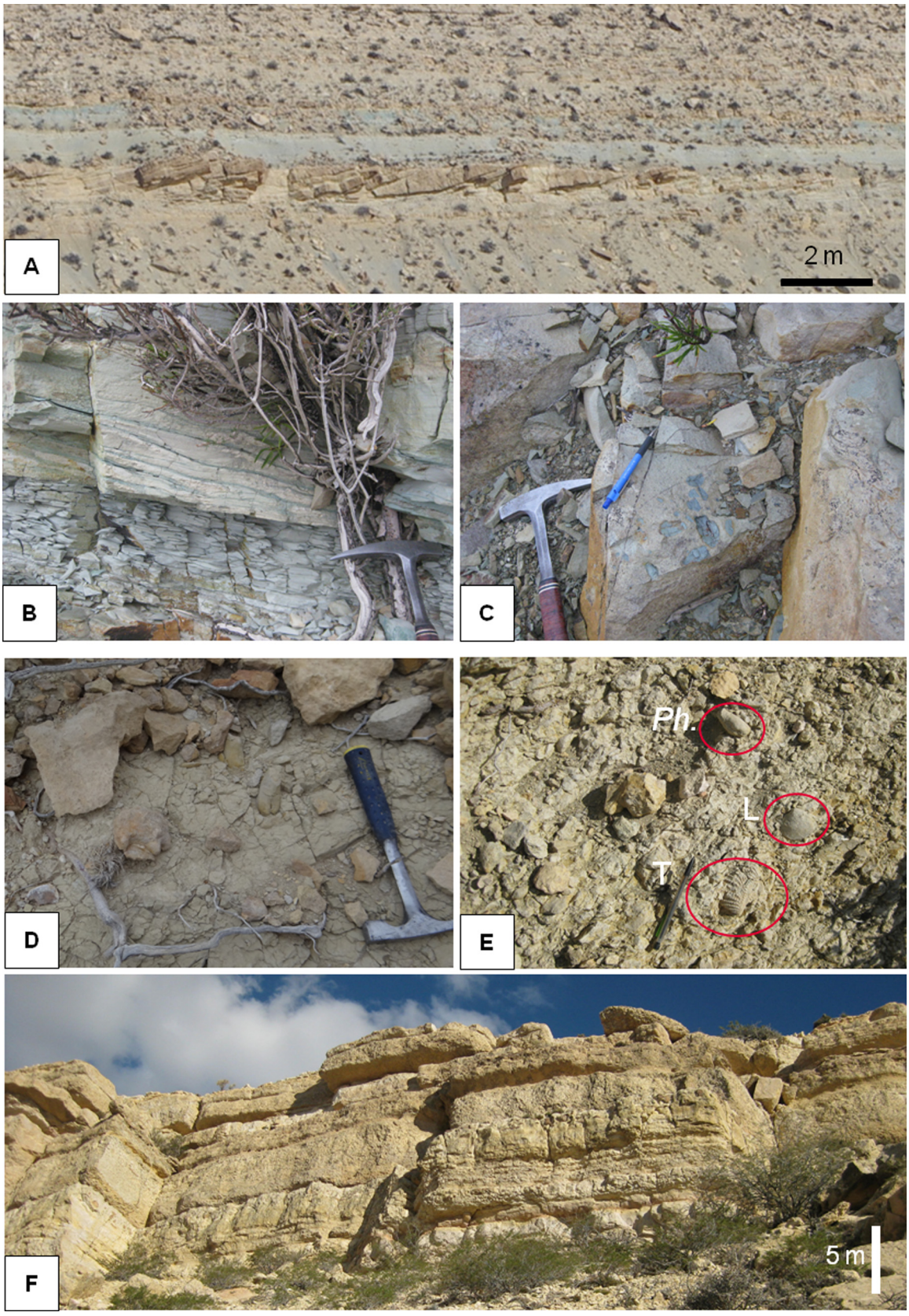

Fig. 8. (A) to (C) Illustration of F.A. 9. (A) General view of sigmoidal cross-bedded sandstones (F.A. 9); (B) Vertical passage from lenticular bedding to wavy bedding; (C) Mud clasts in sandy bed of F.A. 9; (D) and (E) Pholadomya (*Ph.*), Trigoniids (T) and Lucinidea (L) of F.A. 11; (F) Meter-scale laminated limestone beds of F.A. 13.

the foresets, and some beds locally have rippled top surfaces. These sand-rich units are interbedded with or overlain by green silty shales (F3) or green fine to very-fine-grained sandstones (F15). Scarce bivalve fragments are observed.

Interpretation: Cross-bedded sandstones with mud drapes are characteristic of tidal dunes in the intertidal to subtidal zone (Dalrymple 1992, 2010). Episodic changes in the hydrodynamic regime lead to the formation of ripples and mud drapes (Allen, 1980), and therefore a tidal influence is likely (Shanley *et al.*, 1992).

In zones of strong tidal currents, conditions are not favorable for benthos colonization, and few animals can live in this setting (Wilson, 1982, 1986). In addition, faunal diversity increases toward areas with smaller bedforms, as well as on the outer shelf where dunes tend to be replaced by small ripples and interbeds with mud laminae (Desjardins *et al.*, 2012). The rare bivalve fragments suggest a high-energy setting. This indicates that the cross-bedded sandstones of facies association 9 may correspond to tidal dunes. Facies association 9 is interpreted to be deposited in a tidal complex, located above fair-weather wave base.

4.1.10 Facies association 10 (F.A. 10)

Description: This facies association is composed of cross-bedded sandstones (F23) interbedded with grey silty shales (F2). Sandstones are medium- to coarse-grained with trough cross-stratification showing an amalgamated aspect. The beds are few decimeters to a meter thick and show planar bases and tops. Some beds exhibit erosive bases and high velocity planar lamination that dip seaward with low angle. Fine-grained intervals correspond to massive grey silty shales (F2).

Interpretation: The amalgamated aspect suggests a high-energy influence. Trough cross-stratified beds associated with planar lamination suggest formation in high-energy environment by the migration of sand dunes in a shoreface environment (Walker and Plint, 1992; Reading and Collinson, 1996). This FA is interpreted to have been deposited in a shoreface setting.

4.1.11 Facies association 11 (F.A. 11)

Description: This facies association is composed of mixed siliciclastic-carbonate (F.A. 11.a) to siliciclastic (F.A. 11.b) beds with abundant shell fragments, interbedded with fine to very-fine-grained facies.

F.A. 11.a is composed of sandy limestones (F16), interbedded with fine to very-fine-grained green sandstones (F15). The sandy limestone beds are of decimetric to metric thickness and are characterized by sharp bases and tops. They exhibit rare trough cross-stratification. Fossils are abundant and correspond commonly to trigoniids and other bivalves at the tops of the sandy limestone beds. A few bioturbation structures are also observed. F.A. 11.b is composed of alternations of massive sandstones (F17) and green shales (F3). The decimetric to metric sandstone beds display a thickening-upward trend. They are characterized by sharp bases and tops. Fossils are abundant and correspond to fragments of trigoniids, pholadomyiids (Fig. 8D and E), other bivalves and scarce ammonites.

Interpretation: The abundance of shell fragments is an indicator of high-energy. The interlayering of sandstones/sandy limestones with fine to very-fine-grained intervals suggests spatial and temporal variations in the intensity of current induced by wave action (Sweet and Knoll, 1989). The occurrence of trough cross-stratification suggests migration of current-generated bedforms in an extensive shallow subtidal environment (Jiang *et al.*, 2003). Facies association 11 is interpreted as having been deposited in a subtidal environment subject to sustained high-energy conditions.

4.1.12 Facies association 12 (F.A. 12)

Description: This facies association is composed of lenticular units of sandstones or sandy limestones (F18 and F19) with green shaly interbeds (F3). Sandstones (F19) can reach a thickness of five meters when they are organized as a set. They exhibit erosive bases and flat tops. Sandstones are interbedded with green shales (F3). The sandy limestones (F18) reach two meters in thickness in the central part of lenticular units. They show erosive bases, while their tops are sharp and tabular. They are dominantly massive with planar lamination at the top. Bivalves fragments occur at the base and/or the top of the beds. These units are overlained by green shales (F3).

Interpretation: The lenticular units with erosive bases represent a channel filling. The occurrence of shell fragments is an indicator of high-energy. Alternating sandstones and sandy limestones and the abrupt transition to green shales suggest frequent rapid variations in current strength (Reineck and Singh, 1980; Nio and Yang, 1991). The rare planar laminations suggest changes in the hydrodynamic regime (Allen, 1980) and can be interpreted as subtidal deposits influenced by weak wave and tidal currents (Willis *et al.*, 1999).

4.1.13 Facies association 13 (F.A. 13)

Description: This facies association is dominated by limestones (F20) and minor green very fine-grained marly sandstones to marls (F15). Limestone beds are massive with crude laminations (Fig. 8F). They are decimetric to metric in thickness and display sharp bases and tops. Fossils are abundant, represented essentially by *Lucina* sp., *Pholadomya* sp. and occasional oysters in life position. A mottled aspect is observed, probably linked to bioturbation.

Interpretation: The lack of evidence of wave action in limestones and fine-grained facies suggests deposition in low-energy environments (Jiang *et al.*, 2003). The occurrence of oysters in life position and *Lucina* sp. may indicate very shallow waters in tide-dominated areas (Armella *et al.*, 2007). Facies association 13 is interpreted as having been deposited in a lagoon environment.

4.1.14 Facies association 14 (F.A. 14)

Description: This facies association is composed of siliciclastic (F.A. 15.a) to mixed siliciclastic-carbonate (F.A. 15.b) units containing abundant shell fragments, with fine to very fine-grained interbeds (F15). The siliciclastic units correspond to fossil-rich coarse sandstones (F21) and the mixed siliciclastic-carbonate units to fossil-rich sandy limestones (F22). Both facies are made up of massive, structureless units of decimetric to metric thickness exhibiting sharp bases

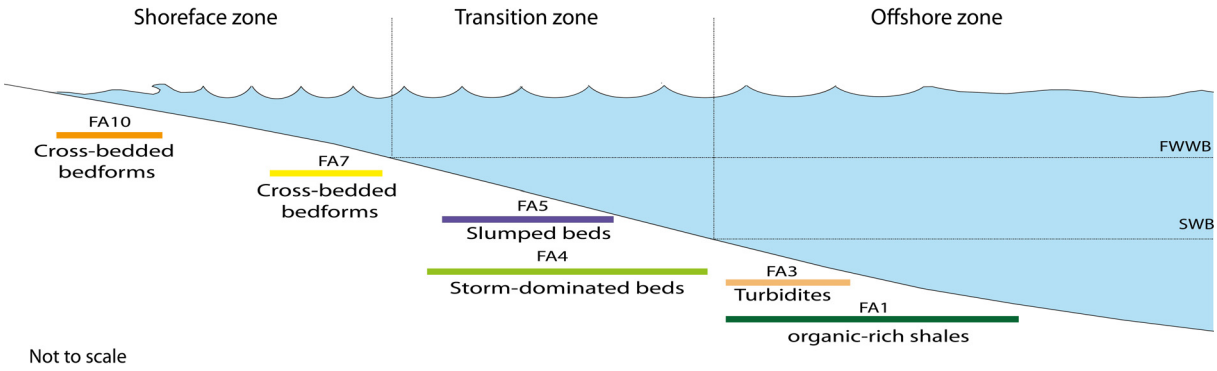

Fig. 9. Schematic profile of a siliciclastic shelf profile showing facies association distribution according to Walker and Plint (1992) zonation, corresponding to distribution occurring in the lower part of the studied interval. The location of the different zones is based on the position of the fair weather wave base (FWWB) and the storm wave base (SWB).

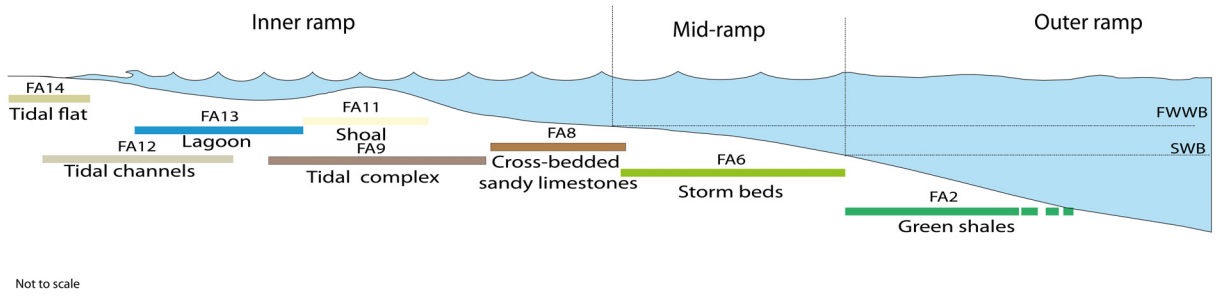

Fig. 10. Schematic profile of a mixed siliciclastic-carbonate ramp showing facies association distribution according to Burchette and Wright (1992), corresponding to facies associations occurring in the upper part of the studied interval (Picún Leufú Formation). The location of the different zones is based on the position of fair weather wave base (FWWB) and the storm wave base (SWB).

and tops and containing bird's-eyes. Fossils are abundant, represented by bivalves and scarce gastropods.

Interpretation: The occurrence of bird's-eye structures indicates that these facies were occasionally exposed above sea level (Pratt *et al.*, 1992). Bird's-eye structures form in supratidal sediments as a result of shrinkage and expansion, gas bubble formation or air escape, and are preserved because of early cementation and filling with calcite, dolomite, evaporite minerals or internal sediment (Shinn 1968, 1983). This facies association is interpreted as a mixed siliciclastic-carbonate tidal flat intersected by channels.

4.2 Depositional environment

Several authors (Mitchum and Uliana, 1985; Spalletti *et al.*, 2000; Zeller, 2013; Kietzmann *et al.*, 2014a) have proposed depositional models for the Vaca Muerta Formation from studies of different parts of the basin. Based on seismic data in the eastern Neuquén Basin, Mitchum and Uliana (1985) interpreted the sedimentary environment of the Vaca Muerta Formation as representing basinal to slope deposits in the Neuquén Embayment. The sedimentary environment of the Vaca Muerta Formation in southern Mendoza was recently studied in details and interpreted as representing the basinal to middle ramp facies of a homoclinal ramp system (Kietzmann *et al.*, 2014a).

Spalletti *et al.* (2000) studied the Vaca Muerta Formation in the Picún Leufú Anticline and proposed a ramp depositional system, in contrast with Zeller (2013) who interpreted these deposits as a mixed shelf to basinal succession.

Based on the investigation of the Picún Leufú Anticline, the stratigraphic distribution of the fourteen facies associations described in the study area suggests two depositional models: the first model corresponds to a siliciclastic shelf (Fig. 9) and the second to a mixed siliciclastic-carbonate ramp (Fig. 10). Similar results were proposed in the Sierra Vaca Muerta (north of the Huincul Ridge) by Kietzmann *et al.* (2014c) who also recognized two depositional systems evolving from clastic to carbonate shallow system.

In the present study, the shelf terminology used is adopted from Walker and Plint (1992) and the ramp terminology from Burchette and Wright (1992).

Walker and Plint (1992) defined the following depositional environments:

- an offshore setting below the storm wave base;
- an offshore transitional zone between the storm wave base and the fair weather wave base;
- shoreface located above the fair weather wave base.

The latter environment is characterized by wave and current agitated hydrodynamic processes.

The first depositional system of the studied succession (Fig. 9) is characterized by two major zones corresponding to shoreface and offshore (*s.l.*) environments, respectively.

The distal deposits are represented by F.A. 1 and correspond to an offshore environment. This sector is

dominated by the settling out of mud and silts. Anoxic to suboxic conditions hindered the proliferation of benthic organisms. Facies association F.A. 4 was deposited in an offshore transitional environment corresponding to episodic, short-lived, high-energy conditions alternating with longer periods of lower energy conditions (fine-grained intervals). During storm periods, material can be transported from shallow to deeper waters.

The shoreface environment is represented by F.A. 7 and F. A. 10, including various facies, reflecting complex hydrodynamic processes with mixed oscillatory and unidirectional flow regimes.

Even if it is difficult to identify paleocurrent structures on the outcrop, the absence of direct connection between these sedimentary bodies and possible continental source allows us to propose a depositionnal environment characterized by processes dominated by the swash and backwash of breaking waves as well as onshore, longshore and rip currents. The sand deposits of F.A. 7 suggest transport and re-sedimentation generated probably by storms (Aurell and Badenas, 1994) and/or longshore currents that entrain and transport sediments (Beer and Gorsline, 1971; Herzer and Lewis, 1979; Lewis and Pantin, 2002; Puig *et al.*, 2003; Normark *et al.*, 2006). Rip currents can also be invoked in the transport of sediments (Dumas and Arnott, 2006). These currents have the potential for transporting coarse sediments from the beach zone to distal areas. They are related to circulation cells and depend primarily on alongshore variations of wave height (Shepard *et al.*, 1941; Goldsmith *et al.*, 1982) leading to sand accumulation in the lower shoreface zone.

Furthermore, some evidence is observed of gravity-driven events. F.A. 3 and F.A. 5 correspond, respectively, to turbidite and slump deposits in the offshore zone (*s.l.*). They are probably due to the downslope collapse of sediments following sand accumulation related to longshore currents on the lower shoreface. This collapse phenomenon is due to instability in shallower areas, resulting from tectonic activity, seismicity or sediment oversteepening (Zakaria *et al.*, 2013).

The second depositional system of the studied succession corresponds to a mixed siliciclastic-carbonate ramp. Burchette and Wright (1992) defined:

- the outer ramp below the storm wave base;
- the mid-ramp between the storm wave base and the fair weather wave base;
- the shoreface located above the fair weather wave base.

The latter environment includes high-energy environments (shoreface and beach) and infratidal to supratidal environments such as lagoon and tidal flats.

The second depositional system of the studied succession is characterized by three zones: inner, middle, and outer ramp (Fig. 10), respectively. The inner ramp includes tidal flat, lagoon, tidal complex, and shoal facies associations. The mixed sedimentary material (siliciclastic and carbonate) in this zone suggests a near but unidentified continental source on the outcrop (siliciclastic flux supplied by the wind or rivers). In the lagoon (F.A. 13), the shallow water and low-energy conditions favour the deposition of limestones and development of Lucinidae. The tidal deposits correspond to tidal channels (F. A. 12) and a tidal complex (F.A. 9). The cross-bedded sandstones of F.A. 8 and F.A. 9 and the bivalve fragments of F.A. 9 indicate high-energy conditions produced by tidal processes (no evidence of wave-influenced morphology). The shoal facies belt (F.A. 11) corresponds to a high-energy environment. This belt was dissected by channels and acted as a barrier restricting water circulation and the development of lagoonal facies further inshore. The middle ramp corresponds to F.A. 6. Abundant bivalve fragments and mud clasts suggest storm influence. Finally, the outer ramp corresponds to F.A. 2, where we can invoke settling out of sediment from suspension in a low-energy environment below storm wave base.

5 Geochemistry and clay-mineral assemblages

5.1 Clay mineralogy

The clay-mineral assemblages are dominated by smectite and kaolinite (Fig. 11). Illite accounts for always less than 20% of the total clay-mineral assemblage. While chlorite is mostly absent, it nevertheless shows peaks in some cases (*e.g.*, samples #19 = 22%, #22 = 12%, #45 = 30%, #48 = 23%), and mixed-layer clay minerals are only present at the top and base of the section (Fig. 11). Smectite and kaolinite abundances are inversely correlated. Smectite shows a major increase in relative abundance above the basal two samples (at about 4 m), jumping from $< 10\%$ to $> 50\%$. Relative smectite abundances then continue to rise until sample #40 (about 270 m, top of the dark-shale interval in the section), but become more scattered toward the top of the section (top of carbonate cycle in regressive systems tract), being close to 100% in the topmost samples. This general up-section increase is accompanied by an evolution in the smectite mineralogy from montmorillonite at the base to saponite at the top. Kaolinite does not show any mineralogical evolution, occurring as the dickite polytype throughout the section. The stratigraphic evolution of the clay mineralogy shows that smectite progressively substitutes for kaolinite from around 150 m in the log section (sample #26, base of shelf sequence in regressive systems). Kaolinite can be interpreted as an inherited mineral or as a clay mineral formed during periods of marked hydrolysis on land, whereas smectite is typical of milder conditions of weathering (*e.g.*, Chamley, 1989 and references therein). Thus, the question is whether the stratigraphic evolution of the clay-mineral assemblage results from changes through time of 1) a single source of clays affected by climate conditions evolving from strongly to mildly hydrolyzing, or 2) clay sources that gradually evolved depending on the emergent land areas being eroded.

5.2 Geochemistry

The chemical index of alteration or CIA reflects the degree of transformation by weathering of alumino-silicate minerals (Nesbitt, 2003): $CIA = 100 \times Al_2O_3 / (Al_2O_3 + Na_2O + K_2O + CaO^*)$, where the calculation is based on molar proportions and CaO^* represents the fraction of CaO associated only with silicates (*i.e.*, here, the non-carbonate fraction). Primary minerals (showing little or no alteration) have a CIA of about 50 or less, whereas secondary clay minerals have CIA values of 75 or more. The CIA is a quantitative measure of the amount of chemically weathered materials contained in a siliciclastic sediment or rock, and reflects the intensity of

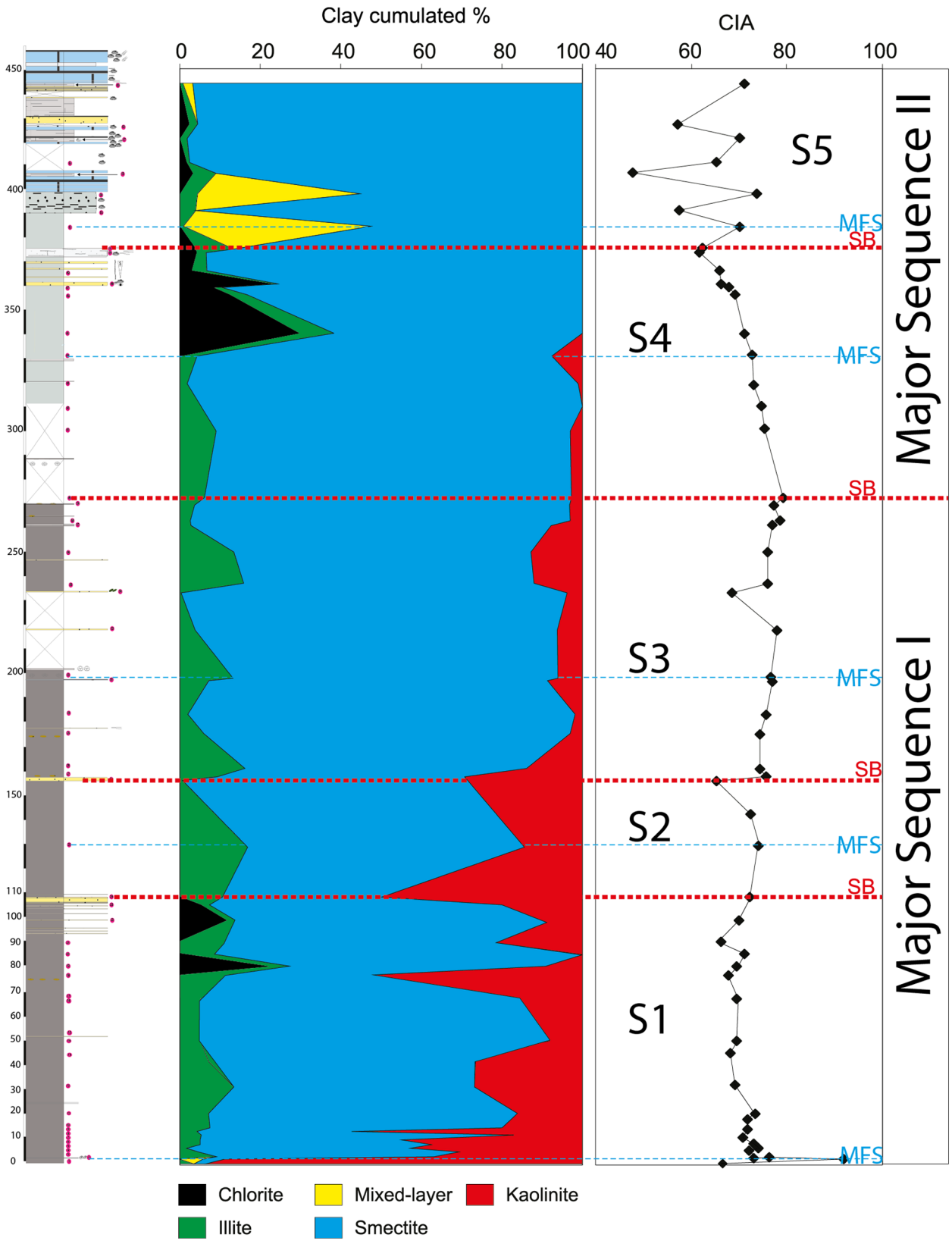

Fig. 11. Relative abundance of clay minerals in clay-size fraction (%) and Chemical Index of Alteration (CIA) (%) in log #3 of the Picún Leufú Anticline. The major subdividing boundaries (SB: sequence boundary; MFS: maximum flooding surface) are established by correlation, according to the sequence stratigraphic framework (See Fig. 14).

chemical weathering in the source areas (Nesbitt and Young, 1982, 1989; Nesbitt, 2003). Here, the CIA values (Fig. 11) indicate that samples from the base of the section up to sample #39 (270 m; dark shales) are dominantly composed of secondary clay minerals, whereas the samples #40 to #51 (272–375 m; green shales) display a clear-cut trend toward lower values. Samples from the topmost carbonate-bearing part of the section (above #59) show scattered values. The stratigraphic evolution of the clay-mineral assemblages does not follow accurately the same trend as that of the CIA. However, from 0 to 330 m, the values of CIA are roughly ranging between 70 and 80 (corresponding to warm and humid conditions according to Nesbitt and Young, 1982, 1989) and are consistent with the presence of kaolinite. Then from 330 m to the top of the section, the values decrease significantly (even with scattering) and range between 50–70 (arid climate condition; Nesbitt and Young, 1982, 1989). The values of CIA show a decrease during the upward transition from dark shales to green shales, with a scattered distribution in the carbonate-bearing top of the section. The CIA value reflects the degree of chemical alteration and transformation of the (source) rocks. Any decrease in CIA could therefore reflect changes in weathering on emergent land areas associated with less intense hydrolyzing conditions. On the other hand, such a decrease could also reflect changes in the source(s) of the detrital flux (Nesbitt and Young, 1982; Young and Nesbitt, 1999). However, the overall progradation of the sedimentary sequence and increasing proportion of sandy facies could also account for the decrease of CIA upwards through the studied section.

5.3 Trace elements

When considering enrichment factors, we observe that the basal sample (#1) is unique in that it shows very high enrichments in several trace elements (As, Mo, Pb and Zn) and noticeable enrichments in U and Sb (Tab. 2). Samples #2 to #40 (lower part of the section) are characterized by a marked enrichment in Mo, and to a lesser degree As and Sb, while U shows weak to detectable enrichment, and V yields weak enrichment. Conversely, samples #41 to #59 (upper part of the section, within carbonate cycles) do not show any interpretable enrichments in the elements mentioned above. In addition, Ni, Cu and Ba that are paleoproductivity proxies (see discussion in Tribovillard *et al.*, 2008 and references therein) show no interpretable enrichment for the entire sample set.

Sample #1 (located at the bottom of the section) displays marked enrichment in TOC and redox-sensitive trace elements (Tab. 2), but no enrichment in productivity proxies (Ba, Ni, Cu). These features reflect reducing conditions in an oxygen-deprived depositional environment, with no indication of strong productivity (Tribovillard *et al.*, 2006). Thus, organic-matter preservation should be attributed to the absence of dissolved oxygen (probable euxinic conditions). Samples #2 to #40 (above the ammonite horizon) have higher enrichment factors in Mo than in U. Moreover, on the U *vs.* Mo diagram (Fig. 12) proposed by Algeo and Tribovillard (2009), these samples plot in the field typical of the particulate iron shuttle (for details about the particulate shuttle process see: Crusius *et al.*, 1996; Dellwig *et al.*, 2010; Scholz *et al.*, 2013; Jilbert and Slomp, 2013). Briefly, dissolved chemical species present in seawater can easily bind onto the Fe and Mn oxy-hydroxides forming particles in the oxidizing part of the water column, thus becoming incorporated in a reversible way. During settling, Fe and Mn oxy-hydroxides can scavenge significant amounts of Mo (Crusius *et al.*, 1996; Little *et al.*, 2015). The oxy-hydroxides can in turn bind settling particles or flocs of OM, or be adsorbed onto clay minerals. Once deposited, the oxy-hydroxides can be chemically reduced leading to release of the previously scavenged ions. These ions can then become solubilized at the sediment-water interface or released into pore waters. In the latter case, they can be incorporated into diagenetic mineral phases (sulphides, carbonates, silicates, etc.). The Mo present in the samples studied here was originally scavenged by Fe- (and probably Mn-) oxy-hydroxides in an oxic water column. After deposition, Mo was released into pore waters through reductive dissolution of the oxy-hydroxides. However, this Mo was trapped in the sediments by incorporation into (*s.l.*) or absorption onto iron sulfides (*e.g.*, pyrite). Thus, the sediments are enriched in Mo, but not (or very slightly) in U, because the latter element is not sensitive to the particulate shuttle. This interpretation is reinforced by the absence of a marked enrichment in V, which also indicates that bottom water conditions were not reducing. However, even if the water column was oxic, the fact that Mo was retained within the sediments indicates that reducing conditions developed at shallow depth below the sediment-water interface; otherwise, Mo would have escaped back into the water column together with pore waters during incipient sediment compaction.

The Mo-rich samples also show enrichments in As and Sb. Co-enrichment in Mo, As and Sb has already been observed associated with the particulate shuttle (Tribovillard *et al.*, 2013, 2015; see discussion in Li *et al.*, 2014). The present study further supports the idea that a co-enrichment in Mo, As and Sb, but with no marked enrichment in U and V, is the signature of the iron shuttle process.

The samples from the top part of the section (#41 to #59) show no significant authigenic enrichment in trace elements, which suggests deposition in fully oxygenated seawater.

6 Stratigraphic sequences and correlations

In the description of sections presented here, we use the concepts of sequence stratigraphy developed by Embry and Johannessen (1992) (transgressive-regressive sequence). A depositional sequence is considered as the record of a cycle of relative sea-level fluctuation, and is made up of two superposed units: the transgressive systems tract (TST) and the regressive systems tract (RST). Deepening trends are considered to indicate a TST, while shallowing-upward trends are interpreted as a RST. The top of a deepening (transgressive) sequence is interpreted as a maximum flooding surface (MFS), while the top of the regressive unit is considered as a sequence boundary (SB). The offshore facies of the TST corresponds to a maximum flooding zone (MFZ).

In the Picún Leufú Anticline, two prograding trends are identified with a regional boundary corresponding to the transition between the grey shale interval and the first occurrence of green shales (Fig. 13). Based on these observations and on the evolution of facies associations,

Table 2. TOC, clay mineralogy and trace element analyses of the Picún Leufú Anticline section (Log #3).

Samples	Altitude (m)	TOC (%)	Smectite (%)	Mixed-layer (%)	Illite %	Kaolinite (%)	Chlorite (%)	Smectite and Mixed-layer types	CIA	As (ppm)	Ba (ppm)	Cu (ppm)	Mo (ppm)	Ni (ppm)	Pb (ppm)	Sb (ppm)	U (ppm)	V (ppm)	Zn (ppm)
1	0.3	24.53	3	0	3	94	0	1	66.7	62.44	331.7	62.12	195.8	109.5	2792.0	1.821	15.39	554.1	9631
2	2	0.04	5	6	0	89	0	0	92.0	9.266	85.96	1	2.558	5.19	26.0	0.1	2.858	10.44	98.91
3	4	7.67	54	0	9	37	0	1	73.0	12.8	224.3	46.26	45.45	20.43	73.5	1.343	7.728	407.1	509
4	5.5	0.08	65	0	5	31	0	2	76.4	8.89	97.1	15.35	13.06	25.92	27.3	0.608	3.776	105.8	15.53
5	6.7	5.69	55	0	2	43	0	2	72.1	9.115	244.4	32.35	37.81	13.68	22.2	1.771	6.504	313.1	54.4
6	11.6	0.98	57	0	5	38	0	1	74.2	9.784	168.8	17.53	42.46	32.19	22.3	0.815	4.425	142.1	101.1
7	12.4	0.25	50	0	5	45	0	1	73.0	10.84	265.7	21.21	23.73	41.41	19.2	1.089	5.166	147.8	50.59
8	13.6	1.83	78	0	5	17	0	1	72.2	13.7	317.8	32.32	26.58	29.38	30.8	1.45	6.996	231.8	31.59
9	15.1	4.38	38	0	4	57	0	1	71.8	11.35	677.5	31.04	50.33	21.69	19.6	1.91	7.809	356.1	21.36
10	17.4	3.18	73	0	7	20	0	1	70.6	17.25	469.3	27.69	124.9	28.16	28.8	1.248	9.458	219.7	31.44
11	20	1.21	77	0	7	16	0	1	72.1	19.56	351.3	27.49	44	25.84	21.7	1.176	6.097	212.3	31.86
12	31	5.6	60	0	13	27	0	1	71.7	15.02	313.4	34.62	127.1	29.64	17.3	2.237	13.73	369	42.1
13	45.9	1.25	66	0	7	27	0	1	73.6	6.076	319.6	19.73	22.66	27.57	21.4	0.668	7.402	143.8	26.07
14	50.9	1.44	87	0	5	8	0	1	72.5	11.15	304.9	23.56	54.82	35.41	22.1	1.103	8.941	147.1	37.26
16	68	6.16	79	0	5	15	0	1	72.0	7.945	307.6	22.57	95.35	39.48	16.3	1.435	11.88	341.8	70.73
18	76	3.26	46	0	11	43	0	1	72.9	13.16	317.7	25.22	89.64	21.57	24.7	1.431	9.962	332.8	186.8
19	80.1	0.03	73	0	2	4	22	3	69.1	3.475	405.6	10.14	1.377	7.376	9.0	0.269	2.521	44.02	18.64
20	85.6	2.12	92	0	8	0	0	3	69.6	6.277	279.3	19.16	31.97	23.14	7.4	1.757	7.082	180.2	246.3
21	90	2.17	68	0	10	23	0	1	72.0	12.14	353.6	13.12	20.13	23.74	26.2	1.005	5.065	146.6	27.21
22	100	0.03	77	0	2	9	12	2	66.2	12.19	399.2	11.72	1.318	24.08	12.8	0.414	1.809	37.5	16.89
23	108	0.02	73	0	2	20	5	3	69.7	3.005	331	21.34	1.448	6.901	11.2	0.279	1.994	35.31	14.81
24	109	0.56	36	0	12	52	0	1	74.1	15.96	350.7	24.68	43.79	16.06	31.4	1.292	5.226	129.4	31.72
25	130.6	0.39	68	0	17	15	0	1	72.4	10.24	340.6	19.91	48.91	14.69	17.1	1.09	6.17	198.1	89.12
26	157	0.01	44	0	1	56	0	4	65.4	2.959	439.9	1	2.847	7.577	10.9	0.259	1.917	28.61	15.68
27	158	0.07	61	0	9	29	0	3	75.6	2.344	233.6	5.142	5.236	10.02	5.6	0.1	1.283	20.09	21.29
28	161	0.49	70	0	16	14	0	1	74.4	10.07	289.2	21.57	23.04	19.11	12.9	0.882	5.238	144	31.38
29	176	0.52	91	0	6	3	0	1	74.3	4.141	286.8	15.92	15.54	9.697	28.6	0.751	3.969	83.57	51.18
30	182.2	0.1	96	0	2	2	0	3	75.7	5.648	180.6	9.825	0.882	5.606	11.0	0.319	3.806	30.09	20.96
31	197.2	0.04	84	0	7	9	0	2	76.6	3.03	138.9	1	5.374	12.86	7.0	0.1	1.282	21.98	14.96
32	198	0.55	81	0	13	6	0	1	76.6	14.82	241.8	18.78	29.04	13.24	29.3	0.693	4.962	100.2	84.84
33	217.6	0.08	90	0	4	6	0	3	77.9	2.599	108.4	1	6.499	11.09	4.7	0.1	1.062	17.95	19.31
34	232.6	0.01	96	0	0	4	0	4	68.5	3.815	413.4	5.623	2.87	8.077	14.0	0.26	1.711	26.06	23.87
35	235.6	0.32	72	0	16	12	0	1	76.0	6.646	226.9	17.02	12.24	17.36	17.6	0.507	4.373	81.25	44.06
36	251	0.23	74	0	13	13	0	1	75.9	8.873	246.2	18.91	10.96	16.23	26.2	0.486	2.962	72.23	41.83
37	261	0.08	89	0	3	8	0	4	77.0	4.582	145.7	8.907	8.752	18.1	6.2	0.1	1.463	38.85	41.89
38	263.5	0.08	94	0	3	3	0	4	78.6	13.18	228.3	17.73	35.44	8.032	25.2	0.875	3.895	55.37	202.2
39	269.4	0.07	93	0	4	3	0	4	77.3	4.308	135.9	7.364	9.636	19.24	6.4	0.1	1.547	31.87	27.03

Table 2. (continued).

Samples	Altitude (m)	TOC (%)	Smectite (%)	Mixed-layer (%)	Illite %	Kaolinite (%)	Chlorite (%)	Smectite and Mixed-layer types	CIA	As (ppm)	Ba (ppm)	Cu (ppm)	Mo (ppm)	Ni (ppm)	Pb (ppm)	Sb (ppm)	U (ppm)	V (ppm)	Zn (ppm)
40	272	0.12	91	0	6	3	0	2	79.1	10.5	213.6	18.69	12.35	21.67	19.3	0.595	3.447	66.72	324.8
41	300	0.16	88	0	9	3	0	2	75.5	6.605	264.7	17.5	2.634	13.75	20.0	0.403	2.561	67.87	42.47
42	310	0.05	94	0	6	0	0	4	74.6	4.166	384.4	10.33	2.314	6.994	18.0	0.363	2.419	53.69	23.73
43	320.5	0.04	97	0	2	1	0	4	73.0	4.545	394	10.25	1.431	20.75	18.3	0.326	2.373	48.45	23.72
44	330	0.03	88	0	4	8	0	3	72.8	5.049	852.5	9.88	1.606	8.724	20.7	0.353	2.05	37.16	25.54
45	340	0.08	62	0	9	0	30	3	71.3	9.386	693.1	18.65	2.16	20.69	32.9	0.533	2.211	49.56	34.82
46	355	0.06	83	0	4	0	12	4	69.1	4.386	296	11.22	0.857	7.872	17.6	0.314	2.148	46.84	28.51
47	360	0.04	89	0	2	0	8	4	67.9	5.03	252.5	7.569	1.435	8.871	14.8	0.271	1.717	33.2	20.27
48	361.5	0.05	76	0	2	0	23	3	66.4	6.997	218.2	1	0.947	9.685	11.5	0.286	2.758	23.04	131.8
49	366.7	0.01	93	0	4	0	3	4	65.9	3.068	372.3	9.234	1.339	7.021	16.7	0.27	2.083	45.48	23.73
50	373	0.02	93	0	2	0	4	4	61.8	3.693	314.3	1	0.692	5.345	14.1	0.1	1.069	21.95	1
51	374	0.05	87	0	9	0	4	4	62.3	4.234	97.73	1	0.575	6.953	5.9	0.1	1.714	16.71	863.5
52	384	0.02	52	47	1	0	0	5	70.2	3.265	433	5.907	0.736	1	11.3	0.241	2.797	47.52	34.81
53	390	0.01	96	0	4	0	0	4	57.4	1.89	575.5	1	0.1	1	9.3	0.1	1.295	24.91	1
54	397	0.02	55	40	4	0	0	5	73.6	1	418.8	22.71	0.1	8.201	6.3	0.779	2.154	84.74	56.67
55	406	0.05	91	0	6	0	3	4	47.9	6.248	575.1	5.722	1.471	6.654	13.9	0.257	5.649	35.27	17.62
56	410	0.06	98	0	1	0	2	5	65.4	4.122	292	1	1.149	8.1	11.9	0.271	3.729	33.64	13.14
57	421	0.05	98	0	2	0	0	5	70.1	4.744	287.6	5.926	0.719	9.151	9.4	0.1	4.272	34.93	17.66
58	427	0.04	96	0	2	0	2	5	57.2	1	1014	1	0.1	1	5.8	0.1	1.831	24.08	26.45
59	443	0.05	97	3	1	0	0	5	71.1	8.26	393.7	15.81	0.819	1	11.9	0.25	2.05	54.94	1

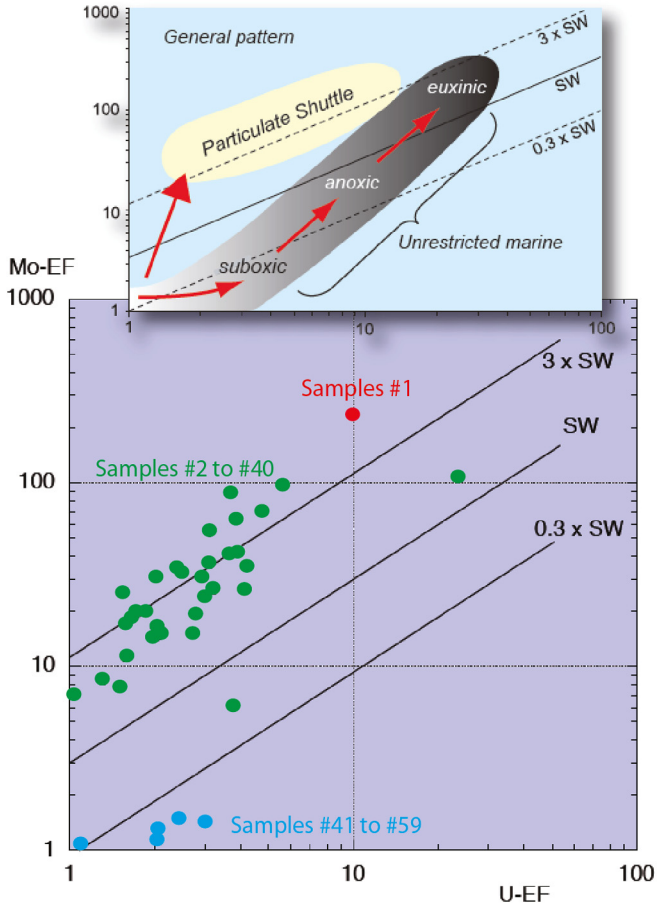

Fig. 12. U–EF *vs.* Mo–EF crossplot of samples from the Tithonian-Berriasian. The top inset diagram illustrates the general patterns of U–EF *vs.* Mo–EF covariation in modern marine environments. The grey field represents "unrestricted marine" environments, characteristic of the eastern tropical Pacific, whereas the yellow field represents the "particulate shuttle" trend, characteristic of depositional systems such as the Cariaco Basin, where intense redox cycling of metal oxyhydroxides (especially Mn-bearing) occurs within the water column. XEF = [(X/Al)sample/(X/Al)PAAS], and X and Al stand for the weight concentrations of element X and Al, respectively. Samples are normalized against the post-Archean average shale (PAAS) compositions of Taylor and McLennan (1985). The trace-element distribution indicates that Sample #1 recorded peculiar, probably euxinic, conditions of deposition, while samples #2 to 40 recorded conditions of depositions under oxic waters and with reducing conditions developing at shallow depth below the sediment-water interface. Samples #41 to 59 recorded fully oxygenated, normal-marine conditions of depositions.

two orders of depositional sequences are recognized (Fig. 14): the higher rank sequences are termed "major T-R sequences", while smaller-scale (high frequency) sequences are simply called "sequences".

6.1 North Picún Leufú sector

"Major T-R sequence I": This sequence marks the base of the deep water facies of the Vaca Muerta Formation. The stacking pattern corresponds to a thin TST and a one hundred meters thick RST. The TST is represented by grey silty shales that overlie the continental deposits of the Tordillo Formation. The total organic content of these shales reaches 24.5% (sample #1, log #3), which corresponds to the highest value recorded. The TST varies in thickness, but remains less than 10 m in this part of the basin. The upper boundary of this TST is marked by a major surface correlated across the Picún Leufú Anticline (Early Tithonian according to Leanza, 1980; Leanza and Zeiss, 1990, 1992), and corresponds to an ammonite-rich horizon interpreted as a condensed interval. In its lower boundary, the TST can be erosive as described by Freije *et al.* (2002) and lies directly above the continental Tordillo Fm. The RST corresponds to fine-grained deposits deposited after the transgression of the early Tithonian (Spalletti *et al.*, 2000). The RST is represented by offshore facies (F.A. 1, 3, 4, and 5) of the Vaca Muerta Formation. The RST varies in thickness from 220 meters in the east to 280 meters in the west. The top of the RST corresponds to shoreface sandstones (F.A. 7) and a transition to green shales (F.A. 2).

This "Major T-R Sequence" contains three higher frequency sequences (Fig. 14) described in the following from the base to the top.

Sequence 1: This sequence is represented at its base by the thin TST described above and is bounded at its top by the ammonite-rich horizon that corresponds to an MFS (Fig. 14). The RST is essentially composed of the offshore silty grey shales (F.A. 1) with rare distal storm related sandstone beds at the base of the section, whose number increases towards the top of the sequence (F.A. 4). The top of this sequence corresponds to the occurrence of turbidites (F.A. 3). The interval corresponding to sequence 1 is correlated between the eight sections. The overall evolution of sequence 1 (Fig 14) shows a general shoaling upward, with its thickness varying from 100 meters (log #3 and 5) to 130 meters (log #7).

Sequence 2: The base of these sequence corresponds to a transition to deeper facies (offshore silty grey shales) interpreted here as a flooding surface. The TST marks a deepening trend and varies from 15 (log #6) to 30 meters (other logs) in thickness. The maximum flooding surface is placed at around the level of the maximum shale content. The overlying RST exhibits a general shallowing trend with the occurrence F. A. 4 and F.A. 7 at its top (tempestites of the offshore transitional zone to shoreface deposits) towards the west (log #8), whereas the eastern section logs show a gradual substitution of these facies associations by F.A. 5 (slumped facies, log #6 to #1, Fig. 14). The thickness of the RST varies from 15 to 40 meters. Sequence 2 does not exceed a thickness of 70 meters and shows more abundant sandstone beds toward the west, while it becomes thinner toward the east with evidence of slumping. The thickness trend associated to the occurrence of slumps (in the west) induced by a destabilization probably related to a tectonic origin suggests a gently prograding geometry (Fig. 14).

Sequence 3: The base of sequence 3 is picked out at the transition from shoreface sandy facies (RST of sequence 2) (F. A. 7) to offshore silty grey shales (F.A. 1) (TST of sequence 3), and is interpreted as a flooding surface in the western part of the Picún Leufú Anticline (log #7 and 8) (Fig. 14). In the eastern part of the anticline (logs 1 to 6), the base of sequence 3 corresponds to the transition from slumped facies (F.A. 5) to offshore silty grey shales (F.A. 1). The general trend is marked

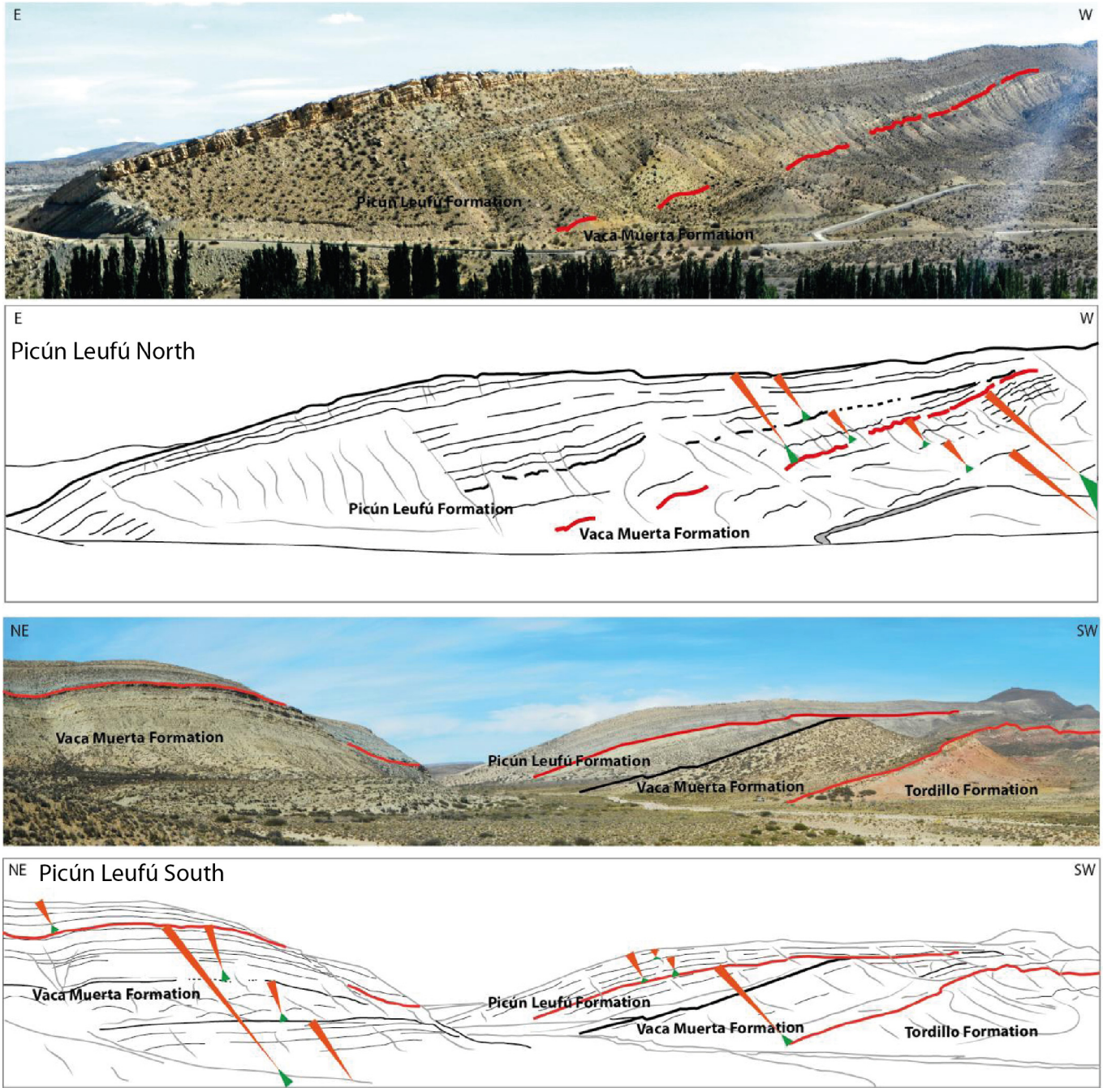

Fig. 13. Panoramic view and line drawing of the major T-R sequences and high-frequency T-R sequences in the north and south Picún Leufú Anticline. The southern part of the Picún Leufú Anticline exposes the most proximal facies of the siliciclastic shelf. This facies corresponds to cross-bedded sandstones attributed to the shoreface environment.

by the increasing thickness of sandstone-rich intervals toward the top of the sequence (Fig. 14) The TST is composed of dominantly silty shales of F.A. 1 and subordinate storm beds (F.A. 4) toward the east (log #1 to 5). The thickness of the TST varies from 10 to 60 m and decreases from 60 m in the west to 10 m in the east, except for log #3 that shows the thickest TST of this sequence (Fig. 14). The MFZ is placed in the interval with the maximum shale content. In some section logs (#4 and 5), the MFZ coincides with horizons containing septarian concretions. The RST corresponds to an enrichment in sand content with the occurrence of shoreface deposits (F.A. 7) at the top. The thickness of the RST varies from 55 to 100 meters, increasing from the west to the east, except in log #3 which shows the thickest RST of this sequence. The top of this sequence corresponds to the top of the "major T-R sequence I" and marks the transition to the green shale deposits.

Major T-R sequence II: This sequence coincides with the first occurrence of the green silty shales of F.A 2. The TST and RST are exposed in the eight logs. The base of the TST is made up of green silty shales and the MFZ is interpreted at the

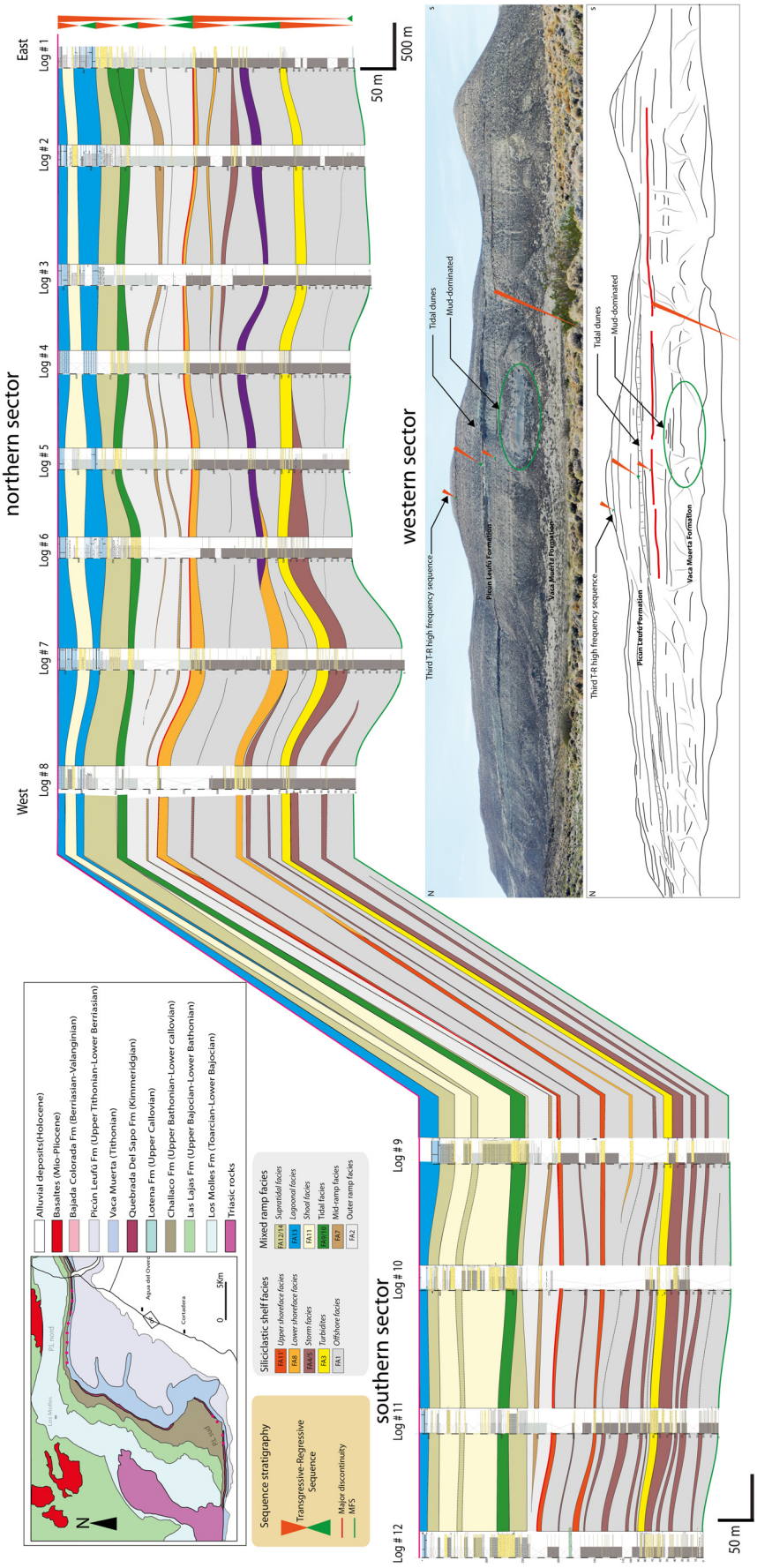

Fig. 14. Correlation diagram of the Tithonian-Berriasian interval of the Picún Leufú Anticline. Correlation is based on key markers shown on satellite images, sequence stratigraphy and facies distribution. The western sector shows a mud-dominated T-R Major Sequence I and exposes the third T-R high-frequency sequence of the second major T-R sequence.

maximum shale content. The RST is a mixed carbonate-siliciclastic sequence with a coarsening-upward stacking pattern. The top of the RST is marked by pure carbonates of F.A. 13 along with the development of a hardground surface encrusted by siliceous sponges (Zeller, 2013), observed in the study area. This hardground marks the base of the next major transgressive-regressive sequence exposed on the back of the anticline but which is not discussed further in this study.

In the second major T-R sequence, two higher order transgressive-regressive sequences can be recognized. The correlation of the different measured sections shows a general aggrading pattern (Fig. 14).

Sequence 4: This sequence starts with the first occurrence of the green silty shales of F.A. 2 and varies in thickness from 60 to 120 meters from west to east (Fig. 14). The TST is recognized by a deepening of depositional environments from the shoreface (F.A. 7 of sequence 3) to the outer ramp (F.A. 2). The TST is covered (vegetation, scree) in three logs (#3, 6 and 8). In the other logs, the top of the TST corresponding to the maximum flooding zone is defined as the interval of maximum shale content. The RST shows a gradual increase in the development of sand beds, which evolve towards the top of the sequence into thick inner ramp proximal deposits with tidal influence (F.A. 8 and F.A. 9). The top of the sequence corresponds to an unconformity observed at outcrop and on high-resolution photographs (Fig. 14). It corresponds to a basal erosional unconformity truncating the tidal deposits.

Sequence 5: This sequence comprises heterogeneous deposits and is marked by the development of lagoonal pure carbonates (F.A. 14). The TST is clearly visible only in the western part of the study area (log #7 and 8), where it is represented by the green silty shales of F.A. 2 (Fig. 14). In the eastern part of the northern flank of the Picún Leufú Anticline, the TST is not well developed. When the TST is identified, the maximum flooding zone is placed at around the maximum shale content. The RST is well developed and varies in thickness from 50 (log #8) to 100 meters (log #6), with an average thickness of 80 meters. The major difference in thickness between log #8 and log #6 is due to erosion of the top of the cliff. The RST is represented by shallow mixed siliciclastic-carbonate deposits (shoal [F.A. 11], tidal channel [F.A. 12] and tidal flat [F.A. 14] facies) that evolve into lagoonal pure carbonates (F.A. 13) at the top.

6.2 South Picún Leufú sector

"Major T-R sequence I": This sequence also marks the beginning of the deep water facies of the Vaca Muerta Formation, corresponding to black and grey silty shales. It corresponds to a thin TST and a thick RST. The upper boundary of the TST corresponds to the ammonite-rich horizon described in the north sector. The RST is represented by F.A. 1, 3, 4 and 10, with a basal ammonite-rich horizon. The RST varies in thickness from 220 meters in the east to 280 meters in the west. The top of the RST is marked by upper shoreface sandstones (F.A. 10) and a transition to green shales (F.A. 2).

This "major T-R sequence" contains three higher frequency sequences, which are described from the base to the top as follows:

Sequence 1: This sequence has an ammonite-rich horizon at its base (MFS). The RST is composed of offshore silty grey shales (F.A. 1) and becomes rapidly enriched by tempestite sands (F.A. 4). The top of this sequence corresponds to the occurrence of F.A. 3 (turbidites). This interval is correlated between the four cross-sections in this sector and also in the northern part of the study area. As in the north sector, the overall evolution of sequence 1 (Fig. 14) shows a general shallowing-upward pattern.

Sequence 2: The TST displays a deepening trend and is 15 meters in thickness. It is mainly composed of silty grey shales. The maximum flooding zone is placed at around the maximum shale content. The RST varies from 15 to 40 meters in thickness, marking a general shallowing trend with the occurrence of F.A. 4 and 10 at the top (tempestite sands to upper shoreface sands) (Fig. 14). Sequence 2 is generally isopachous and does not reach 90 meters

Sequence 3: The base of sequence 3 is picked out at the transition from shoreface sands (F.A. 10) to offshore silty grey shales (F.A. 1). The TST is composed dominantly of silty shales of F.A. 1 with scarce tempestites (F.A. 4).The TST is 10 meters in thickness. The MFZ is placed at around the maximum shale content. The RST corresponds to relative upward enrichment in sand content with the occurrence of shallower facies (F.A. 10) towards the top. The RST varies from 40 to 60 meters in thickness. The top of this sequence corresponds to the top of "major T-R sequence I" and marks the transition to the green shale deposits (Fig. 14).

Major T-R sequence II: This sequence also coincides with the first occurrence of the green silty shales of F.A. 2 in this part of the Picún Leufú Anticline. The base of the TST is made up of green silty shales and the MFZ is interpreted at the maximum shale content. In this sector, the RST is also composed of mixed carbonate-siliciclastic deposits. The top of the RST is marked by pure carbonates (F.A. 13) with the development of a hardground surface encrusted by siliceous sponges.

In this major T-R sequence, two higher order transgressive-regressive sequences are recognized. The correlation of the four measured sections shows a general aggrading pattern (Fig. 14). It corresponds to an erosional unconformity truncating the tidal deposits.

Sequence 4: This sequence starts with the first occurrence of the green silty shales of FA 2 and varies from 60 to 120 meters in thickness from west to east. The TST is recognized by the facies deepening from shoreface deposits (F. A. 8 of sequence 3) to outer ramp deposits (F.A. 2). The TST is covered (vegetation, scree) on three logs (#3, 6 and 8). In the other logs, the top of the TST that corresponds to the maximum flooding zone is defined as the interval of maximum shale content. The RST shows a gradual development of sand beds which evolve to the top of the sequence into thick proximal deposits of the inner ramp with tidal evidence (F.A. 9 and F. A. 10). The top of the sequence corresponds to the unconformity observed on the high-resolution photography. It corresponds to an erosional unconformity truncating the tidal deposits.

Sequence 5: The sequence is marked by the development of lagoonal carbonates (F.A. 13). In this sector, the TST is thick and corresponds to shoal sands and the MFS is not clearly defined. The RST is well developed and is represented by shallow mixed siliciclastic-carbonate deposits that evolve towards lagoonal carbonates at the top (Fig. 14).

In the Picún Leufú Anticline, the Major T-R sequence I show a general shallowing-up trend, with higher order deepening-up represented by offshore facies and shallowing-up represented by shoreface facies. The western outcrops (Fig. 14) shows more mud-dominated intervals than in the north, whereas the southern part of the Picún Leufú Anticline shows more sand-rich facies than the other sectors. In Major T-R sequence II, most of the TST is represented by F.A. 2 without any clear evidence of a retrogradational stacking pattern. The RST is marked by high carbonate content. The western flank of the Picún Leufú Anticline (Fig. 14) shows a third high-frequency T-R sequence.

The five higher-order T-R depositional sequences allow us to determine the geometry of the depositional profile as follows (Fig. 14):

- subhorizontal surfaces associated with offshore deposits, interpreted as forming a gently sigmoidal pattern in the case of sequence阗
- slightly inclined surfaces and a pronounced sigmoidal geometry for sequences 2 and 3 with a major event (slumping) at the top of sequence 2 and thick prograding sands in sequence 3;
- a general aggrading pattern with steep surfaces associated with the development of tidal deposits in sequence 4 and a more horizontal pattern for sequence 5.

Indeed, the lateral thickness variability and absence of any general trend suggest a pre-depositional topography inherited from the Tordillo Formation (Fig. 14). The initial transgressive surface seems to be whereas the lateral variability from south to north across the Picún Leufú anticline can be explained by different sedimentation rates in the proximal and the distal areas.

7 Discussion

7.1 Stratigraphic pattern

Two Major Sequences can be highlighted from facies analysis and sequence stratigraphy of the Vaca Muerta-Picún Leufú Formations in the Picún Leufú Anticline (northern and southern flanks). The first sequence is dominated by siliciclastics with shelf morphology (Walker and Plint, 1992), whereas the second sequence is composed of mixed siliciclastic-carbonate deposits with ramp morphology (Burchette and Wright, 1992).

The lower interval of the Vaca Muerta Fm. (Major Sequence I) is characterized by the occurrence of sand bodies in the distal shoreface, the development of slumps on the slope and deposition of turbidites further offshore (Fig. 15). The sandy accumulations formed in the distal part of the shoreface by longshore currents have the potential to serve as storage zones for the supply of sediments to distal areas. The slumps and turbidity flows could have originated from shallower domains; destabilization of material on the slope would be followed by basinward transport of sediment and the deposition of turbidites (Fig. 16).

The stratigraphic position of the shoreface sand bodies (F.A. 7), slumps (F.A. 5) and turbidites (F.A. 3) highlights the sequence boundary (Fig. 14). A relationship is proposed between these facies, processes of initiation of destabilization and the sea-level fluctuations. A fall in relative sea level during deposition of the regressive system tract (equivalent of the LST in Exxon's model) can create favorable conditions for destabilization of the shoreface zone leading to the basinward formation of slumps and turbidites (Posamentier and Martinsen, 2011). Other mechanisms could be invoked, such as a major increase in sedimentation rate. During deposition of the second interval (Major Sequence II), the sedimentary environment of the Vaca Muerta Fm. evolved toward a mixed siliciclastic-carbonate ramp. Zeller (2013) studied the transition between Vaca Muerta and Picún Leufú Formations in detail in the northern flank of Picún Leufú Anticline, and describing a mixed siliciclastic-carbonate sequence with less abundant pure carbonate facies compared to the Major Sequence II defined here. The lower part of Major Sequence II shows an overall progradational pattern. It begins with a transgressive period leading to deeper conditions with the deposition of outer ramp green shales (F.A. 2), followed by shallower conditions with the accumulation of tidal deposits. The upper part of Major Sequence II is associated with the development of shoal facies and lagoonal carbonates on the inner ramp in a more aggradational context.

7.2 Sea-level changes and tectonic control

The Tithonian to Berriasian-Valanginian interval over most of the basin is interpreted as the result of a second-order eustatic cycle, combined with persistent regional subsidence regulated by cooling and thermal contraction phenomena. The much-reduced clastic sediment supply is associated with condensed sedimentation under anaerobic-dysaerobic conditions (Legarreta and Gulisano, 1989; Legarreta and Uliana, 1991, 1996; Legarreta *et al.*, 1993; Doyle *et al.*, 2005).

Biostratigraphic data from the southern part of the basin show that the studied interval is Tithonian-Early Berriasian in age (Leanza, 1973, 1980; Leanza and Zeiss, 1990, 1992). The Vaca Muerta Formation was deposited from the lower Tithonian (*Virganosphinctes mendozanus* biozone) to the middle Tithonian (base of *Windhauseniceras interspinosum* biozone) and the Picún Leufú Formation from the upper Tithonian (base of *Windhauseniceras interspinosum* biozone) to the lower Berriasian (lower part of *Substeueroceras Koeneni* zone).

In the Neuquén Embayement (central part of the basin), Mitchum and Uliana (1985) studied the Tithonian-Valanginian interval from seismic sections and defined ten depositional sequences correlated with the trend of eustatic sea-level changes.

The basin fill geometry has been correlated with eustatic changes and three geometrical groups can be defined. The Tithonian-Berriasian interval studied by Mitchum and Uliana (1985) was correlated to the eustatic curve (Vail *et al.*, 1982). It covers more than six sequences with generally sigmoidal geometry (dated Early to Middle Tithonian: A, B, C) and oblique geometry (dated Late Tithonien-Berriasien: D, E, and F).The sigmoidal pattern indicates moderate aggradation and progradation, whereas the oblique pattern corresponds to low aggradation and high progradation (Mitchum and Uliana, 1985).

The sequences and geometric pattern defined by Mitchum and Uliana (1985) cannot be directly correlated with our

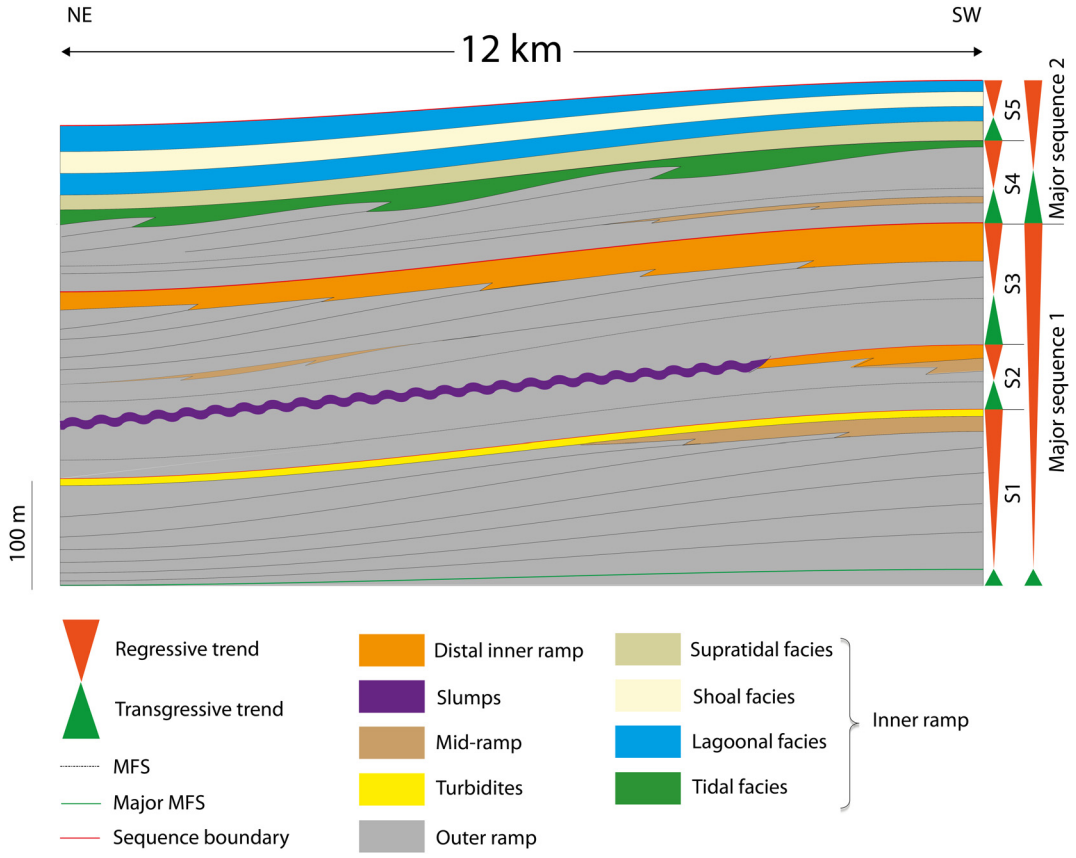

Fig. 15. Synthetic view of the Tithonian-Berriasian stacking pattern in the Picún Leufú Anticline based on sequence stratigraphic framework.

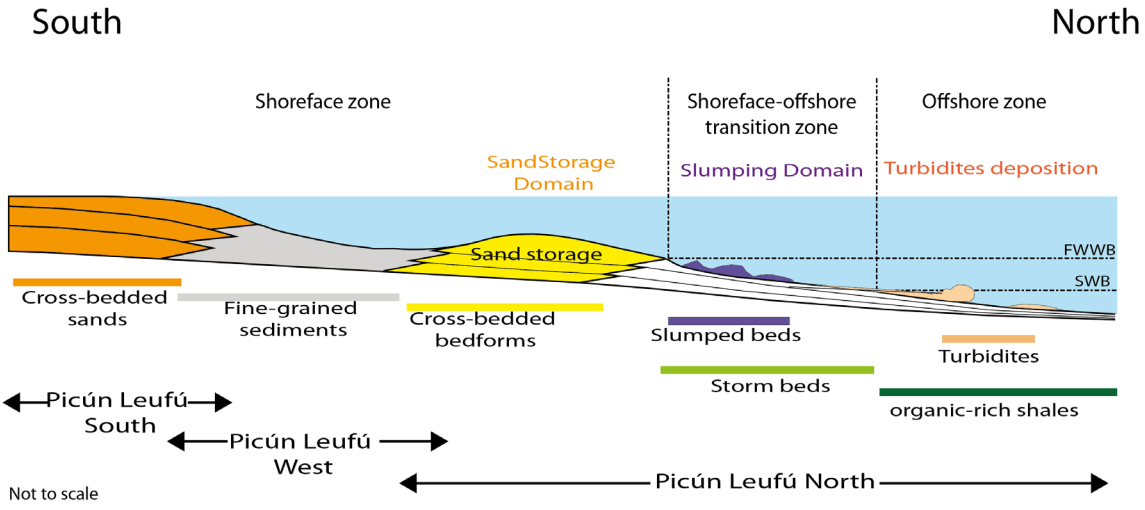

Fig. 16. Interpretative shelf profile and facies association distribution extended to the Picún Leufú depocentre. The profile is exaggerated to highlight sand storage on the lower shoreface zone.

sequences and geometric patterns because of the different methods used for delineating sequence boundaries (seismic *vs.* outcrop) and the different geological context due to the presence of the Huincul Ridge.

The concordance between the geometric pattern of Mitchum and Uliana (1985) and the global coastal encroachment curve (Vail *et al.*, 1982) suggests that this model can be applied partially to the Tithonian-Berriasian interval of the Picún Leufú Anticline.

Consequently, sequences 1, 2 and 3 can be correlated with sequence set A, B and C of Mitchum and Uliana (1985), indicating a moderate rise of sea level, whereas sequences 4

and 5, which indicate a weak aggradation could be correlated with a part of the sequence set D, E and F in seismic line.

Tectonics can play a role in determining facies and sequence architecture. Hallam *et al.* (1991) and Spalletti *et al.* (2000) evoke the role of regional tectonics related to the growth of the magmatic arc in the development of the Tithonian-Berriasian succession in the southern part of the basin. The proximity of the Huincul Ridge to the Picún Leufú Anticline affected the facies distribution of the studied interval. The role of the Huincul Ridge has been specified by Spalletti *et al.* (2000), who suggested that this positive structure favoured the development of tidally-dominated sediments in shallow environments corresponding in this study to the deposits of major T-R sequence II. However, evidence of slumped facies during the deposition of the major T-R sequence I suggests an uplift that impact the sedimentary environment probably earlier than suggested by Spalletti *et al.* (2000). The confinement of the deposit area during deposition of the lower part of the Vaca Muerta Formation probably favoured the development of transverse marine currents and a zone of sand storage in shallow environments.

Besides, several authors (Eppinger and Rosenfeld, 1996; Spalletti *et al.*, 2008; Naipauer *et al.*, 2012) have studied the provenance of the Vaca Muerta Formation sediments, concluding that there was two source areas: the magmatic arc in the west and the North Patagonian Massif in the south. These authors consider the western magmatic arc as the main source during sea-level lowstands (Eppinger and Rosenfeld, 1996; Spalletti *et al.*, 2008; Naipauer *et al.*, 2012]. This interpretation is somewhat doubtful in view of the vicinity of the North Patagonian Massif. However, our study fails to identify any sedimentary processes related to a fluvial source.

7.3 Paleoenvironments

The progressive evolution of the clay mineral assemblages (smectites substituting for kaolinite), as well as the transformation of smectite minerals from montmorillonite to saponite may be interpreted in two different ways:

- changes in the weathering affecting emergent lands under less intense hydrolyzing conditions;
- a change of sediment source area (Chamley, 1989).

Although CIA values and clay mineralogy both suggest a change to less intense hydrolyzing conditions and/or a change in the detrital source toward the top of the section, their diachronous stratigraphic evolution indicates a difference in the signal recorded by the CIA and the clay mineralogy. It should be kept in mind that the clay fraction of the sediments studied here represents only a minor proportion of the total clastic material compared to the silt fraction. Consequently, some variation may affect the clay-fraction composition with no detectable impact on the record of the CIA that is influenced by a much larger part of the clastic supply. The CIA is more sensitive to alteration of feldspars in the silt fraction that dominates over the clay fraction in the present case.

The stratigraphic variations of the clay-mineral assemblages are not in phase with the sequence-stratigraphy evolution tuned to sea-level variations. Although not completely unequivocal, this observation suggests that the nature of the clay-mineral assemblage does not depend on the (re-) mobilization of sediment volumes induced by sea-level variations. Instead, we conclude that the clay-mineral assemblages record climate changes occurring on land.

The paleogeographical and paleoclimatological reconstructions of the lower Cretaceous indicate that the Neuquén Basin was located between latitudes 42° S and 50° S (Spalletti *et al.*, 1999), at the boundary between two climatic provinces: arid to the north and warm temperate to the south, with a seasonal rainfall pattern (Cuneo, 2003; Sagasti, 2005). Notably, based on astronomical cycle records, Sagasti (2005) proposed that, during the Lower Cretaceous, sedimentation in the Neuquén Basin was affected by latitudinal migration of the climatic belts. By analogy, we can conclude that, during the Tithonian-Berriasian interval, latitudinal migration of these climatic belts caused fluctuations in sedimentary environments and siliciclastic/carbonate supply. Under warm temperate climatic conditions, the southern part of the Neuquén Basin was subject to seasonal rainfall, which provoked chemical weathering and high runoff. These factors favoured conditions of hydrolysis leading to kaolinite formation and the transport of erosion by-products towards the basin. This configuration allowed the development of a siliciclastic supply. In contrast, during periods of less intense hydrolysis indicated by lower CIA values and absence of kaolinite, the reduced terrigenous supply led to a relative increase in carbonate production and the development of a mixed siliciclastic-carbonate ramp.

In addition to (or apart from) climate evolution, the decreasing intensity of hydrolysing conditions may be related to a decrease in the amount of drainage on emergent land masses. Such modifications in the drainage system could be ascribed to geomorphological changes possibly linked to the regional-scale tectonic regime.

7.4 Oxygenation status of the southern Neuquén Basin

7.4.1 Redox conditions

As discussed above, the trace-element analyses indicates that sample #1 records peculiar conditions of deposition, which were probably euxinic, while samples #2 to 40 record conditions of deposition in oxic waters, with reducing conditions developing at shallow depth below the sediment-water interface, or episodically above it (Fig. 12 shows that one sample diverges from the group it belongs to and indicates more strongly reducing conditions). Samples #41 to 59 are indicative of fully oxygenated, normal-marine conditions of deposition. In addition to the oxygenation status of the basin, the degree of restriction of deep-water circulation may also be assessed. The restriction of deep-water circulation can influence authigenic U–Mo enrichment of marine sediments. All other variables being equal, restricted circulation lowers the degree of trace element enrichment in sediments owing to a decreased input of aqueous trace metal species supplied to the basinal water mass from the global ocean (Algeo and Lyons, 2006; Little *et al.*, 2015). However, water-mass restriction is often correlated with other environmental variables such as reduced

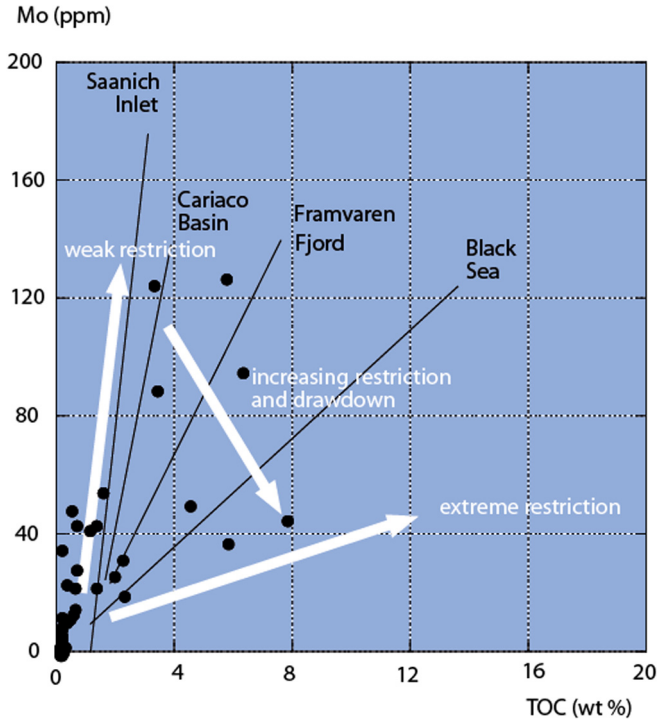

Fig. 17. Total organic carbon content *vs.* Mo concentration ([TOC] *vs.* [Mo]) diagrams for samples from the Tithonian-Berriasian interval. The solid lines represent four present-day basins characterized by restriction of water mass circulation. The degree of restriction increases from the Saanich Inlet to the Black Sea. See explanations given in Algeo and Lyons (2006) and Algeo *et al.* (2007). The four reference settings (Saanich Inlet, Cariaco Basin, Framvaren Fjord and Black Sea) are characterized by increasing water mass restriction due to hydrological conditions. This limits the replenishment of dissolved Mo coming from the open sea, which may lead to exhaustion of this element in the case of massive scavenging from the water column down to the sediment. The samples with the highest TOC values straddle fields on the diagram reflecting increasing restriction and dissolved-Mo drawdown. The TOC-enriched samples are located in the lower part of the section, which tends to indicate that the depositional environment underwent episodic restriction of water mass circulation during deposition of the lower part of the Vaca Muerta Formation.

redox conditions (especially within the suboxic–anoxic redox range), which may enhance trace metal uptake and offset the effects of increased restriction (Algeo and Lyons, 2006). A TOC *vs.* Mo diagram (Algeo and Lyons, 2006; Algeo *et al.*, 2007) has been designed to visualize the degree of paleo-water mass restriction (Fig. 14).

This diagram is based on the analysis of some well-known present-day environments, which are used as references (Algeo and Lyons, 2006; Algeo *et al.*, 2007). We observe a dominant "Saanich Inlet-type" distribution, suggesting moderate water mass restriction. However, the samples with the highest TOC values straddle fields on the diagram that reflect increasing restriction and dissolved-Mo drawdown (Fig. 17). These samples suggest deposition under marked water mass restriction. They are located in the lower part of the studied section, which suggests that the sedimentary environment underwent episodic limitation of water mass circulation during deposition of the lower part of the Vaca Muerta Formation.

8 Conclusion

Our study bring additional sedimentological and geochemical data that allows us to propose an alternative for the Tithonian-Berriasian interval exposed in the southern part of the Neuquén Basin. We are able to characterize the vertical evolution of successive facies belts, representing siliciclastic and mixed ramp environments.

We propose the development of a siliciclastic shelf with storm and turbidity flows during deposition of the lower part of the Vaca Muerta Formation, changing to a mixed siliciclastic-carbonate ramp with tidal influence during deposition of the upper part of the Vaca Muerta Formation.

Based on the identification of shallowing and deepening cycles, the Tithonian-Berriasian interval corresponds to two major transgressive-regressive sequences and five high-frequency transgressive-regressive sequences.

The high-frequency transgressive-regressive sequences correspond to three progradational sequences, one aggradational-progradational sequence and an aggradational sequence.

The variation of CIA and clay mineralogy in the stratigraphic column show that climate evolution is well recorded by sedimentary environments during the Tithonian-Berriasian interval.

Trace element analyses suggest that the southern part of the Neuquén Basin was not an open marine environment but instead corresponded to a platform or ramp with episodic and moderate limitation of marine circulation, at least during the onset of deposition of the Vaca Muerta Formation. This restriction of water mass circulation was probably due to the existence of a topographic high, corresponding to the Huincul Ridge, which hindered mixing with the open marine environment. Thus, geochemical characterization of the southern Neuquén Basin setting during the Tithonian-Berriasian interval suggests the presence of:

- "normal marine" conditions with oxic sea waters and pore waters rapidly turning to suboxic at shallow depth below the sediment-water interface;
- an episodically limited circulation pattern, at the onset of deposition the Vaca Muerta Formation.

Overall, the moderate organic matter enrichment of the Vaca Muerta Formation in the southern part of the Neuquén Basin appears mainly related to basin restriction.

Acknowledgments. This paper is a synthesis of the PhD studies of the first author, undertaken at the university of Pau et des Pays de l'Adour (France) and sponsored by TOTAL S.A. The authors thank TOTAL S.A. for permission to publish this paper. M.S.N. Carpenter post-edited the English style and grammar. We would like to thank the reviewers S. Rohais and B. Bomou for their constructive review.

References

Aguirre-Urreta B, Lazo DG, Griffin M, Vennari VV, Parras AM, Cataldo C, *et al.* 2011. Megainvertebrados del Cretácico y su

importancia bioestratigráfica. In: Leanza HA, Arregui C, Carbone O, Danieli JC, Vallés JM, eds. *Geología y Recursos Naturales de la Provincia del Neuquén*. Buenos Aires: Asociación Geológica Argentina, pp. 465–488.

Aigner T. 1982. Calcareous tempestites: storm-dominated stratification in Upper Muschelkalk limestones (Middle Trias, SW-Germany). In: Einsele G, Seilacher A, eds. *Cyclic and event stratification*. Berlin: Springer-Verlag, pp. 180–198.

Algeo TJ, Lyons TW. 2006. Mo-total organic carbon covariation in modern anoxic marine environments: implication for analysis of paleoredox and hydrographic conditions. *Paleoceanography* 21: PA1016. DOI: 10.1029/2004PA001112.

Algeo TJ, Rowe H. 2012. Paleoceanographic applications of trace-metal concentration data. *Chemical Geology* 324–325: 6–18.

Algeo TJ, Tribovillard N. 2009. Environmental analysis of paleoceanographic systems based on molybdenum-uranium covariation. *Chemical Geology* 268: 211–225.

Algeo, TJ, Lyons WL, Blakey RC, Over DJ. 2007. Hydrographic conditions of the Devono-Carboniferous North American Seaway inferred from sedimentary Mo-TOC relationships. *Palaeogeography, Palaeoclimatolology, Palaeoecolology* 256: 204–230.

Allen JRL. 1980. Sand waves: a model of origin and internal structures. *Sedimentary Geology* 26: 281–328.

Allen JRL. 1982. Structures and sequences related to gravity-current surges. In: *Sedimentary Structures. Their Character and Physical Basis*. Amsterdam: Elsevier, Chapter 10, pp. 395–431.

Armella C, Cabaleri N, Leanza HA. 2007. Tidally dominated rimmed-shelf facies of the Picún Leufú Formation (Jurassic/Cretaceous boundary) in southwest Gondwana, Neuquén Basin, Argentina. *Cretaceous Research* 28: 961–979.

Aurell M, Badenas B. 1994. Factors controlling the sedimentary evolution of the kimmeridgian ramp in the north iberian basin (NE Spain). *Estudios Geologicos* 50: 91–101.

Beer RM, Gorsline DS. 1971. Distribution, composition and transport of suspended sediment in Redondo submarine canyon and vicinity (California). *Marine Geology* 10: 153–175.

Behar F, Beaumont V, De B Penteado HL. 2001. Technologie Rock-Eval 6 : performances et développements. *Oil & Gas Science and Technology – Rev. IFP* 56 (2): 111–134.

Boersma JR, Terwindt JHJ. 1981. Neap-spring tide sequences of intertidal shoal deposits in a mesotidal estuary. *Sedimentology* 28: 151–170.

Bomou B, Adatte T, Tantawy AA, Mort H, Fleitmann D, Huang Y, *et al.* 2013. The expression of the Cenomanian-Turonian oceanic anoxic event in Tibet. *Palaeogeography Palaeoclimatology Palaeoecology* 369: 466–481.

Bouma AH. 1962. Sedimentology of some flysch deposits: a graphic approach to facies interpretation. Amsterdam: Elsevier, 168 p.

Bout-Roumazeilles V, Cortijo E, Labeyrie L, Debrabant P. 1999. Clay mineral evidence of nepheloid layer contributions to the Heinrich layers in the northwest Atlantic. *Palaeogeography, Palaeoclimatology, Palaeoecology* 146: 211–228.

Brenchley PJ, Pickerill RK, Strombert SG. 1993. The role of wave reworking on the architecture of storm sandstone faces, Bell Island Group (Lower Ordovician), eastern Newfound-land. *Sedimentology* 40: 359–382.

Brumsack HJ. 2006. The trace metal content of recent organic carbon-rich sediments: implications for Cretaceous black shale formation. *Palaeogeography Palaeoclimatology Palaeoecology* 232: 344–361.

Burchette TP, Wright VP. 1992. Carbonate ramp depositional systems. In: Sellwood BW, ed. *Ramps and Reefs. Sedimentary Geology* 79: 3–57.

Carignan J, Hild P, Mevelle G, Morel J, Yeghicheya, D. 2001. Routine analyses of trace element in geological samples using flow injection and low pressure on-line liquid chromatography coupled to ICP-MS: a study of geochemical reference materials BR, DR-N, UB-N, AN-G and GH. *Geostandards Newsletter* 25: 187–198.

Carozzi AV, Orchuela IA, Rodriguez Schelotto ML. 1993. Depositional models of the Lower Cretaceous Quintuco–Loma Montosa Formation, Neuquén Basin, Argentina. *Journal of Petroleum Geology* 16: 421–450.

Chamley H. 1989. Clay sedimentology. Berlin Heidelberg (Germany): Springer-Verlag, 623 p.

Charrier R. 1985. Estratigrafía, evolución tectónica y significado de las discordancias de los Andes chilenos entre 32°S y 36°S durante el Mesozoico y Cenozoico. In: Frutos J, Oyarzún R, Pincheira M, eds. *Geología y Recursos Minerales de Chile*. Concepción: Universidad de Concepción, pp. 101–133.

Cook HE, Taylor ME. 1977. Comparison of Continental slope and shelf environments in the Upper Cambrian and lowest Ordovician of Nevada. *Society of Economic Paleontologists and Mineralogists*, Special Publication 25: 51–81.

Crusius J, Calvert S, Pedersen T, Sage D. 1996. Rhenium and molybdenum enrichments in sediments as indicators of oxic, suboxic, and sulfidic conditions of deposition. *Earth and Planetary Science Letters* 145: 65–78.

Cuneo NR. 2003. Early Cretaceous terrestrial ecosystems from Patagonia: The Baquero Group, a case study. *Abstract of the Geological Society of America Annual Metting 2003, Seattle*. Available from https://gsa.confex.com/gsa/2003AM/finalprogram/abstract_61614.htm.

Dalrymple RW. 1992. Tidal depositional systems. In: Walker RG, James NP, eds. *Facies Models: Response to Sea Level Changes*. Ontario: Geological Association of Canada, pp. 195–218.

Dalrymple RW. 2010. Tidal depositional systems. In: James NP, Dalrymple RW, eds. *Facies Models 4*. Ontario: Geological Association of Canada, pp. 201–232.

Dalrymple RW, Choi K. 2007. Morphologic and facies trends through the fluvial-marine transition in tide-dominated depositional systems: a systematic framework for environmental and sequence-stratigraphic interpretation. *Earth-Science Reviews* 81: 135–174.

Dellwig O, Leipe T, März C, Glockzin M, Pollehne F, Schnetger B, *et al.* 2010. A new particulate Mn-Fe-P-shuttle at the redoxcline of anoxic basins. *Geochimica et Cosmochimica Acta* 74(24): 7100–7115.

Desjardins RP, Buatois LA, Mangano MG. 2012. Tidal flats and subtidal sand bodies. Developments in Sedimentology. Elsevier B.V., vol. 64.

Digregorio JH. 1972. Neuquén. In: Leanza AF, ed. *Geología Regional Argentina*. Córdoba: Academia Nacional de Ciencias, pp. 139–505.

Doyle P, Poiré DG, Spalletti LA, Pirrie D, Brenchley P, Matheos SD. 2005. Relative oxygenation of the Tithonian-Valanginian Vaca Muerta- Chachao formations of the Mendoza Shelf, Neuquén Basin, Argentina. In: Veiga GD, Spalletti LA, Howell JA, Schwarz E, eds. *The Neuquén Basin, Argentina: a case study in sequence stratigraphy and basin dynamics*. London: Geological Society, Special Publication, vol. 252, pp. 185–206.

Dumas S, Arnott RWC. 2006. Origin of hummocky and swaley cross-stratification. The controlling influence of unidirectional current strength and aggradation rate. *Geology* 34: 1073–1076. DOI: 10.1130/G22930A.1.

Embry AF, Johannessen EP. 1992. T–R, facies analysis and reservoir distribution in the uppermost Triassic- Lower Jurassic succession, western Sverdrup basin, Arctic Canada. In: Vorren TO, Bergsager

E, Dahl-Stamnes OA, Holter E, Johansen B, Lie E, Lund TB, eds. *Arctic Geology and Petroleum Potential*. Norwegian Petroleum Society (NPF), Special Publication, vol. 2, pp. 121–146.

Epistalié J, Madec M, Tissot B, Leplat P. 1977. Source rock characterization method for petroleum exploration. *Proceedings of the Offshore Technology Conference, Maggio 2–5, Houston, TX*, pp. 439–444.

Epistalié J, Madec M, Leplat P, Paulet J. 1985. Method and device 633 for determining the organic carbon content of a sample. *U.S. Patent* 4: 519, 983.

Eppinger KJ, Rosenfeld U. 1996. Western margin and provenance of sediments of the Neuquén Basin (Argentina) in the Late Jurassic and Early Cretaceous. *Tectonophysics* 259: 229–244.

Flügel E. 2004. Microfacies of carbonate rocks: analysis, interpretation and application. Berlin: Springer.

Franzese JR, Spalletti LA. 2001. Late Triassic – Early Jurassic continental extension in southwestern Gondwana: tectonic segmentation and pre break-up rifting. *Journal of South American Earth Sciences* 14: 257–270.

Freije H, Azúa G, González R, Ponce J, Zavala C. 2002. Actividad Tectónica Sinsedimentaria en el Jurásico del Sur de la Cuenca Neuquina. *V Congreso de Exploración y Desarrollo de Hidrocarburos. Mar del Plata, 29 de octubre a 2 de Noviembre de 2002*. Actas CD, 17 p.

Friedman GM, Chakraborty C. 2006. Interpretation of tidal bundles: two reasons for a paradigm shift. *Carbonates and Evaporites* 21: 170–175.

Giusiano A, Alonso J, Chebli G, Ibañez G. 2011. Gas no convencional en la cuenca Neuquina. El shale gas en la provincia del Neuquén. Informe de la Subsecretaría de Hidrocarburos, Energía y Minería, Gobierno de la Provincia del Neuquén, 54 p.

Goldsmith V, Bowman D, Kiley K. 1982. Sequential stage development of crescentic bars: Hahoterim beach, southeastern mediterranean. *Journal of Sediment Petrolology* 52: 233–249.

Gradstein FM, Ogg JG, Schmitz MD, Ogg GM. 2012. The geologic time scale. Amsterdam: Elsevier, vol. 1.

Groeber P. 1946. Observaciones geológicas a lo largo del meridiano 70. Hoja Chos Malal. *Revista de la Sociedad Geológica Argentina* 1 (3): 177–208.

Gulisano CA, Gutiérrez Pleimling AR, Digregorio RE. 1984. Análisis estratigráfico del intervalo Tithoniano–Valanginiano (Formaciones Vaca Muerta, Quintuco y Mulichinco) en el suroeste de la provincia de Neuquén. *9° Congreso Geológico Argentino, Actas* 1: 221–235.

Hallam A, Grose JA, Ruffell AH. 1991. Palaeoclimatic significance of changes in clay mineralogy across the Jurassic-Cretaceous boundary in England and France. *Palaeogeography, Palaeoclimatology, Palaeoecology* 81: 173–187.

Herzer RH, Lewis DW. 1979. Growth and burial of a submarine canyon off Motunau, north Canterbury, New Zealand. *Sedimentary Geology* 24: 69–83

Hesse R, Schacht U. 2011. Early diagenesis of deep sea sediments. In: Hueneke H, Mulder T, eds. *Developments in Sedimentology.* Amsterdam (The Netherlands): Elsevier, vol. 63, pp. 557–713.

Howell JA, Schwarz E, Spalletti LA, Veiga GD. 2005. The Neuquén Basin: an overview. In: Veiga GD, Spalletti LA, Howell J, Schwarz E, eds. *The Neuquén Basin: A case study in sequence stratigraphy and basin dynamics*. London: Geological Society, Special Publications, 252, pp. 1–14.

Jiang G, Christie-Blick N, Kaufman AJ, Banerjee DM, RAI V. 2003. Carbonate platform growth and cyclicity at a terminal Proterozoic passive margin, Infra Krol Formation and Krol Group, Lesser Himalaya, India. *Sedimentology* 50: 921–952.

Jilbert T, Slomp CP. 2013. Iron and manganese shuttles control the formation of authigenic phosphorus minerals in the euxinic basins of the Baltic Sea. *Geochimica et Cosmochimica Acta* 107: 155–169.

Kietzmann DA, Palma RM. 2011. Las tempestitas peloidales de la Formación Vaca Muerta (Tithoniano-Valanginiano) en el sector surmendocino de la Cuenca Neuquina, Argentina. *Latin American Journal of Sedimentology and Basin Analysis* 18: 121–149.

Kietzmann DA, Vennari VV. 2013. Sedimentología y estratigrafía de la Formación Vaca Muerta (Tithoniano-Berriasiano) en el área del cerro Domuyo, norte de Neuquén, Argentina. *Andean Geology* 40: 41–65.

Kietzmann DA, Palma RM, Riccardi AC, Martín-Chivelet J, López-Gómez J. 2014a. Sedimentology and sequence stratigraphy of a Tithonian–Valanginian carbonate ramp (Vaca Muerta Formation): a misunderstood exceptional source rock in the Southern Mendoza area of the Neuquén Basin, Argentina. *Sedimentary Geology* 302: 64–86.

Kietzmann DA, Ambrosio A, Suriano J, Alonso S, Vennari VV, Aguirre-Urreta MB, *et al.* 2014b. Análisis sedimentológico y estratigráfico secuencial de las Formaciones Vaca Muerta y Quintuco en el área de Chos Malal, Cuenca Neuquina. *IX Congreso de Exploración y Desarrollo de Hidrocarburos* TT2: 269–288.

Kietzmann DA, Ambrosio A, Suriano J, Alonso S, Vennari VV, Aguirre-Urreta MB, *et al.* 2014c. Variaciones de facies de las secuencias basales de la Formación Vaca Muerta en su localidad tipo (Sierra de la Vaca Muerta), Cuenca Neuquina. *IX Congreso de Exploración y Desarrollo de Hidrocarburos* TT2: 269–288.

Kietzmann DA, Palma RM, Llanos MPI. 2015. Cyclostratigraphy of an orbitally-driven Tithonian–Valanginian carbonate ramp succession, Southern Mendoza, Argentina: implications for the Jurassic–Cretaceous boundary in the Neuquén Basin. *Sedimentary Geology* TT2: 269–288.

Komatsu T, Naruse H, Shigeta Y, Takashima R, Maekawa T, Dang HT, *et al*. 2014. Lower Triassic mixed carbonate and siliciclastic setting withSmithian–Spathian anoxic to dysoxic facies, An Chau basin, northeastern Vietnam. *Sedimentary Geology* 300: 28–48.

Leanza HA. 1973. Estudio sobre los cambios faciales de los estratos limítrofes Jurasico-Cretácicos entre Loncopué y Picún Leufú, provincia del Neuquén, República Argentina. *Revista de la Asociación Geológica Argentina* 28: 97–132.

Leanza HA. 1980. The Lower and Middle Tithonian Ammonite fauna from Cerro Lotena, Province of Neuquén, Argentina. *Zitteliana* 5: 1–49 (München).

Leanza HA. 1981. The Jurassic/Cretaceous boundary beds in west central Argentina and their ammonite zones. *Neues Jahrbuch für Geologie und Paläontologie, Abhandlungen* 161: 62–92.

Leanza HA. 1994. Estratigrafía del Mesozoico posterior a los Movimientos Intermálmicos en la comarca del Cerro Chachil, provincia del Neuquén, Argentina. *Revista de la Asociación Geológica Argentina* 48: 71–84.

Leanza HA, Hugo CA. 1978. Sucesión de amonites y edad de la Formación Vaca Muerta y sincrónicas entre los paralelos 35° y 40° l. s. Cuenca Neuquina-Mendocina. *Revista de la Asociación Geológica Argentina* 32: 248–264.

Leanza HA, Zeiss A. 1990. Upper Jurassic lithostratigraphic Limestone from Argentina (Neuquén Basin): stratigraphy and fossils. *Facies* 22: 169–186.

Leanza HA, Zeiss A. 1992. On the ammonite fauna of Lithostratigraphic Limestones from the Zapala region (Neuquén province, Argentina), with the description of a new genus. *Zentralblat für Geologie und Paläontologie* 6: 1841–1850 (Stuttgart).

Leanza HA, Zeiss A. 1994. The Lithostratigraphic Limestones of Zapala (Central Argentina) and their ammonite fauna. *Geobios* 16: 245–250.

Leanza HA, Marchese HG, Riggi JC. 1978. Estratigrafía del Grupo Mendoza, con especial referencia a la Formación Vaca Muerta, entre los paralelos 35° y 40° l. s. Cuenca Neuquina-Mendocina. *Revista de la Asociación Geológica Argentina* 32: 190–208.

Leanza HA, Hugo CA, Repol D, Salvarredy Aranguren M. 2003. Miembro Huncal (Berriasiano inferior): un episodio turbidítico en la Formación Vaca Muerta, Cuenca Neuquina, Argentina. *Revista de la Asociación Geológica Argentina* 25(2): 248–254.

Leanza HA, Sattler F, Martinez R, Carbone O. 2011. La Formación Vaca Muerta y Equivalentes (Jurásico Tardío–Cretácico Temprano) en la Cuenca. Neuquina. In: Leanza HA, Arregui C, Carbone O, Daniela JC, Vallés JM, eds. *Geología y Recursos Naturales de la Provincia del Neuquén, Neuquén*. Buenos Aires: Asociación Geológica Argentina, pp. 113–129.

Legarreta L. 2002. Eventos de desecación en la Cuenca Neuquina: Depósitos continentales y distribución de hidrocarburos. Mar del Plata. *V Congreso de Exploración y Desarrollo de Hidrocarburos, Mar del Plata, Argentina*. Actas.

Legarreta L, Gulisano C. 1989. Análisis estratigráfico secuencial de la Cuenca Neuquina (Triásico superior-Terciario inferior). In: Chebli G, Spalletti LA, eds. *Cuencas Sedimentarias Argentinas, Serie Correlación Geológica*. San Miguel de Tucumán: Universidad Nacional de Tucumán, vol. 6, pp. 221–243.

Legarreta L, Uliana MA. 1991. Jurassic-Cretaceous marine oscillations and geometry of backarc basin fill, Central argentine Andes. In: Macdonald DI, ed. *Sedimentation, tectonics and eustasy. Sea level changes at active plate margins*. Oxford: International Association of Sedimentologists, Special Publication, vol. 12, pp. 429–450.

Legarreta L, Uliana MA. 1996. The Jurassic succession in west-central Argentina: stratal patterns, sequences and palaeogeographic evolution. *Palaeogeography, Palaeoclimatology, Palaeoecology* 120: 303–330.

Legarreta L, Gulisano C, Uliana MA. 1993. Las secuencias sedimentarias Jurásico-Cretácicas. Relatorío Geología y Recursos Naturales de Mendoza, *XII° Congreso Geológico Argentino y II° Congreso de Exploración de Hidrocarburos*, pp. 87–114.

Lewis KB, Pantin HM. 2002. Channel-axis, overbank and drift sediment waves in the southern Hikurangi Trough, New Zealand. *Marine Geology* 192: 123–151.

Li XL, Shi HM, Xia H-Y., Zhou Y-P., Qiu YW. 2014 Seasonal hypoxia and its potential forming mechanisms in the Mirs Bay, the Northern South China Sea. *Continental Shelf Research* 80: 1–7.

Little SH, Vance D, Lyons TW, McManus J. 2015. Controls on trace metal authigenic enrichment in reducing sediments: insights from modern oxygen-deficient settings. *American Journal of Science* 315: 77–119.

Lowe DR. 1982. Sedimentary gravity flows: II. Depositional models with special reference to the deposits of high-density turbidity currents. *Journal of Sedimentary Research* 52: 279–297.

Macdonald D, Gómez Pérez I, Franzese J, Spalletti L, Lawver L, Gahagan L, *et al*. 2003. Mesozoic break-up of SW Gondwana: implications for regional hydrocarbon potential of the southern South Atlantic. *Marine and Petroleum Geology* 20: 287–308.

Manceda R, Figueroa D. 1995. Inversion of the Mesozoic Neuquén Rift in the Malargüe Fold and Thrust Belt, Mendoza, Argentina. In: Tankard AJ, Suárez Soruco R, Welsink HJ, eds. *Petroleum Basins of South America*. American Association of Petroleum Geologist, Memoir, vol. 62, pp. 369–382.

Marchese HG. 1971. Litoestratigrafía y variaciones faciales de las sedimentitas mesozoicas de la Cuenca Neuquina, Prov. de Neuquén, Rep. Argentina. *Asociación Geológica Argentina Revue* 26: 343–410.

Maretto H, Pangaro F. 2005. Edad de formación de algunas de las grandes estructuras del engolfamiento de la Cuenca Neuquina: actividad tectónica durante la depositación de la Fm. Quintuco. *6° Congreso de exploración y Desarrollo de Hidrocarburos (Mar del Plata)*, CD-ROM, 11 p.

Massaferro JL, Zeller M, Giunta DL, Sagasti G, Eberli GP. 2014. Evolución del sistema mixto tithoniano-valanginiano (Formaciones Vaca Muerta, Quintuco y equivalentes) a partir de estudios de afloramientos y subsuelo, centro- sur de la Cuenca Neuquina. *IX Congreso de Exploración y Desarrollo de Hidrocarburos*.

Mitchum RM, Uliana MA. 1985. Seismic stratigraphy of carbonate depositional sequences. Upper Jurassic/Lower Cretaceous. Neuquén Basin, Argentina. In: Berg BR, Woolverton DG, eds. *Seismic Stratigraphy, II. An Integrated Approach to Hydrocarbon Analysis*. American Association of Petroleum Geologists, Memoir, vol. 39, pp. 255–274.

Mosquera A, Ramos VA. 2006. Intraplate deformation in the Neuquén Embayment. In: Kay SM, Ramos VA, eds. *Evolution of an Andean margin: a tectonic and magmatic view from the Andes to the Neuquén Basin (35°–39° lat)*. Geological Society of America, Special Paper, vol. 407, pp. 97–124.

Mutti E. 1992. Turbidite Sandstones. Instituto di Geologia, Universitaà di Parma, Milan, 275 p.

Naipauer M, García Morabito E, Marques JC, Tunik M, Rojas Vera EA, Vujovich G, *et al*. 2012. Intraplate Late Jurassic deformation and exhumation in western central Argentina: constraints from surface data and U–Pb detrital zircon ages. *Tectonophysics* 524–525: 59–75.

Nesbitt HW. 2003. Petrogegenesis of siliciclastic sediments and sedimentary rocks. In Lentz DR, ed. *Geochemistry of sediments and sedimentary rocks: evolutionary considerations to mineral deposit-forming environments. Geol Assoc Canada GeoText* 4: 39–51.

Nesbitt HW, Young GM. 1982. Early Proterozoic climates and plate motions inferred from major element chemistry of lutites. *Nature* 299: 715–717.

Nesbitt HW, Young GM. 1989. Formation and diagenesis of weathering profiles. *Journal of Geology* 97: 129–147.

Nio SD, Yang C. 1991. Diagnostic attributes of clastic tidal deposits: a review. In: Smith DG, Reinson GE, Zaitlin BA, Rahmani RA, eds. *Clastic Tidal Sedimentology*. Calgary: Canadian Society of Petroleum Geologists, Memoire, vol. 16, pp. 3–27.

Normark WR, Piper DJW, Sliter R. 2006. Sea-level and tectonic control of middle to late Pleistocene turbidite systems in Santa Monica Basin, offshore California. *Sedimentology* 53: 867–897.

Pángaro F, Veiga R, Vergani G. 2002. Evolución tecto-sedimentaria del área de Cerro Bandera, Cuenca Neuquina, Argentina. *5° Congreso Argentino de Exploración de Hidrocarburos, Mar del Plata*, Abstracts on CD.

Parent H, Garrido AC, Schweigert G, Scherzinger A. 2011. The Tithonian ammonite fauna and stratigraphy of Picún Leufú, southern Neuquén Basin, Argentina. *Revue de Paléobiologie* 30: 45–104.

Posamentier HW, Martinsen OJ. 2011. The character and genesis of submarine mass-transport deposits: insights from outcrop and 3D seismic data. In: Shipp RG, Weimer P, Posamentier HR, eds. *Mass-transport deposits in deepwater settings*. Tulsa: SEPM, Special Publication, vol. 96, pp. 7–38.

Pratt BR, James NP, Cowan CA. 1992. Peritidal Carbonates. In: Walker RG, James NP, eds. *Facies Models: Response to Sea*

Level Changes. St. Johns: Geological Association of Canada, pp. 303–322.
Puig P, Ogston AS, Mullenbach BL, Nittrouer CA, Sternberg RW. 2003. Shelf-to-canyon sediment-transport processes on the Eel continental margin (northern California). *Marine Geology* 193: 129–149.
Ramos VA. 1999. Evolución tectónica de la Argentina. In: Caminos R, ed. *Geología Argentina Servicio Geológico Minero Argentino*. Buenos Aires: Anales, vol. 29, pp. 715–784.
Reading HG, Collinson JD. 1996. Clastic coasts. In: Reading HG, ed. *Sedimentary Environments: Processes, Facies and Stratigraphy.* Cornwall: Blackwells, pp. 154–231.
Reineck HE, Singh IB. 1980. Depositional Sedimentary Environments. Berlín- Heidelberg, New York: Springer-Verlag, 549 p.
Reineck HE, Wunderlich F. 1968. Classification and origin of flaser and lenticular bedding. *Sedimentology* 11: 99–104.
Riccardi AC. 2008. The marine Jurassic of Argentina: a biostratigraphic framework. *Episodes* 31: 326–335.
Sagasti G. 2005. Hemipelagic record of orbitally-induced dilution cycles in: Lower Cretaceous sediments of the Neuquén Basin. In: Veiga GD, Spalletti LA, Howell JA, Schwarz E, eds. *The Neuquén Basin, Argentina: a case study in sequence stratigraphy and basin dynamics*. London: Geological Society, Special Publication, vol. 252, pp. 231–250.
Scholz F, McManus J, Sommer S. 2013. The manganese and iron shuttle in a modern euxinic basin and implications for molybdenum cycling at euxinic ocean margins. *Chemical Geology* 335: 56–68.
Shanley KW, Mccabe PJ, Hettinger RD. 1992. Tidal influence in Cretaceous fluvial strata from Utah, USA: a key to sequence stratigraphic interpretation. *Sedimentology* 39: 905–930.
Shepard FP, Emery KO, La Fond EC. 1941. Rip currents: a process of geological importance. *Journal Geology* 49: 337–369.
Shinn EA. 1968. Burrowing in Recent Lime Sediments of Florida and the Bahamas. *Journal of Paleontology* 42 (4): 879–894.
Shinn EA. 1983. Tidal Flat Environment. Carbonate Depositional Environments: AAPG Memoir 33: 172–210.
Spalletti LA, Franzese JR, MacDonald DIM, Gomez Perez I. 1999. Paleogeographic evolution of southern South America during the Cretaceous. *Boletim do 5° Simposio sobre o Cretaceo do Brasil y 1° Simposio sobre el Cretácico de America del Sur, Sao Paulo*, pp. 87–95.
Spalletti LA, Franzese J, Matheos SD, Schwarz E. 2000. Sequence stratigraphy in tidally-dominated carbonate-siliciclastic ramp, the Tithonian of the southern Neuquén Basin, Argentina. *Journal of the Geological Society* 157: 433–446.
Spalletti LA, Colombo Piñol F. 2005. From alluvial fan to playa: an Upper Jurassic ephemeral fluvial system, Neuquén Basin, Argentina. *Gondwana Research* 8 (3): 363–383.
Spalletti LA, Queralt I, Matheos SD, Colombo F, Maggi J. 2008. Sedimentary petrology and geochemistry of siliciclastic rocks from the upper Jurassic Tordillo Formation (Neuquén Basin, western Argentina): implications for provenance and tectonic setting. *Journal of South American Earth Sciences* 25 (4): 440–463.
Sweet K, Knoll AH. 1989. Marine pisolites from Upper Proterozoic carbonates of East Greenland and Spitsbergen. *Sedimentology* 36: 75–93.
Taylor SR, McLennan SM. 1985. The Continental Crust: its Composition and Evolution. Oxford: Blackwell, 312 p.
Tribovillard N, Algeo T, Lyons TW, Riboulleau A. 2006. Trace metals as paleoredox and paleoproductivity proxies: an update. *Chemical Geology* 232: 12–32.
Tribovillard N, Bout-Roumazeilles V, Algeo TJ, Lyons TW, Sionneau T, Montero-Serrano JC, *et al.* 2008. Paleodepositional conditions in the Orca Basin as inferred from organic matter and trace metal contents. *Marine Geology* 254: 62–72.
Tribovillard N, Algeo TJ, Baudin F, Riboulleau A. 2012. Analysis of marine environmental conditions based on molybdenum-uranium covariation – Applications to Mesozoic paleoceanography. *Chemical Geology* 324–325: 46–58.
Tribovillard N, Armynot Du Châtelet E, Gay A, Barbecot F, Sansjofre P, Potdevin J-L. 2013. Geochemistry of cold seepage-impacted sediments: per-ascensum or per-descensum trace metal enrichment? *Chemical Geology* 340: 1–12.
Tribovillard N, Hatem E, Averbuch O, Barbecot F, Bout-Roumazeilles V, Trentesaux A. 2015. Iron availability as a dominant control on the primary composition and diagenetic overprint of organic-matter-rich rocks. *Chemical Geology* 401: 67–82.
Vail PR, Hardenbol J, Todd RG. 1982. Jurassic unconformities and global sea-level changes from seismic and biostratigraphie. *Bulletin of the Houston Geological society (abst.)* 25: 3–4.
Van Der Weijden CH. 2002. Pitfalls of normalization of marine geochemical data using a common divisor. *Marine Geology* 184: 167–187.
Veiga GD, Spalletti LA. 2007. The Upper Jurassic (Kimmeridgian) fluvial-aeolian systems of the southern Neuquén Basin, Argentina. *Gondwana Research* 11: 286–302.
Veiga R, Verzi H, Maretto H. 2001. Modelado bidimensional en el ámbito central de la cuenca Neuquina (Argentina). *Boletín de Informaciones Petroleras XVIII* 67: 50–63.
Vergani GD, Tankard AJ, Belotti HJ, Welsink HJ. 1995. Tectonic evolution and paleogeography of the Neuquén Basin, Argentina. In: Tankard AJ, Suárez Soruco R, Welsink HJ, eds. *Petroleum Basins of South America*. American Association of Petroleum Geologists, Memoir 62, pp. 383–402.
Volkheimer W, Rauhut OWM, Quattrocchio ME, Martinez MA. 2008. Jurassic paleoclimates in Argentina, a review. *Revista de la Asociación Geológica Argentina* 63: 549–556.
Walker RG, Plint AG. 1992. Wave- and storm-dominated shallow marine systems. In: Walker RG, James NP, eds. *Facies Models: Response to Sea Level Change*. Waterloo, Ontario: Geological Association of Canada, pp. 219–238.
Wallace-Dudley K, Leckie D. 1993. The Lower Kaskapau Formation (Cenomanian): a multiple-frequency, retrogradational shelf system, Alberta, Canada. *American Association of petroleum Geologists Bulletin* 77: 414–435.
Weaver, C. (1931). Paleontology of the Jurassic and Cretaceous of west central Argentina. *University of Washington, Seattle, Memoir* 1, 469 p.
Willis BJ, Bhattacharya JP, Gabel SL, White CD. 1999. Architecture of a tide-influenced river delta in the Frontier Formation of central Wyoming, USA. *Sedimentology* 46: 667–688.
Wilson JB. 1982. Shelly faunas associated with temperate offshore tidal deposits. In: Stride AH, ed. *Offshore Tidal Sands*. London: Chapman and Hall, pp. 126–171.
Wilson JB. 1986. Faunas of tidal current and wave-dominated continental shelves and their use in the recognition of storm deposits. In: Knight RJ, McLean JR, eds. *Shelf Sands and Sandstones*. Calgary: Canadian Society of Petroleum Geologists, Memoir 11, pp. 313–326.
Yang CS, Nio SW. 1985. The estimation of palaeohydrodynamic processes from subtidal deposits using time series analysis methods. *Sedimentology* 32: 41–57.
Young GM, Nesbitt WH. 1999. Paleoclimatology and provenance of the glaciogenic Gowganda Formation (Paleoproterozoic), Ontario, Canada: a chemostratigraphic approach. *Geological Society of America Bulletin* 111 (2): 264–274.

Yrigoyen MR. 1991. Hydrocarbon resources from Argentina. *World Petroleum Congress, Buenos Aires. Petrotecnia* 13 (Special issue): 38–54.

Zakaria AA, Howard DJ, Christopher A-LJ, Tongkul F. 2013. Sedimentary facies analysis and depositional model of the Palaeogene, West Crocker submarine fan system, NW Borneo. *Journal of Asian Earth Sciences* 76: 283–300.

Zavala C, Freije H. 2001. Jurassic clastic wedges sourced from the Huíncul Arch. A case study in the Picún Leufú area. Neuquén Basin, Argentina. *AAPG Hedberg Conference. "New Technologies and New Play Concepts in Latin America"*. Mendoza, Argentina, pp. 31–32.

Zavala, C., Maretto, H., Di Meglio, M. (2005). Hierarchy of bounding surfaces in Aeolian sandstones of the Tordillo Formation (Jurassic). Neuquén Basin, Argentina. *Geologica Acta* 3: 133–145.

Zeller M. 2013. Facies, Geometries and sequence stratigraphy of the mixed carbonate-siliciclastic Quintuco-Vaca Muerta system in the Neuquén Basin, Argentina: an integrated approach. *Open Access Dissertations*, Paper 1099.

Zeller M, Eberli GP, Weger RF, Giunta DL, Massaferro JL. 2014. Seismic expressions of the Quintuco – Vaca Muerta system based on outcrop facies and geometry. *IX Congreso de Exploración y Desarrollo de Hidrocarburos*.

Cite this article as: Krim N, Bonnel C, Tribovillard N, Imbert P, Aubourg C, Riboulleau A, Bout-Roumazeilles V, Hoareau G, Fasentieux B. 2017. Paleoenvironmental evolution of the southern Neuquèn basin (Argentina) during the Tithonian-Berriasian (Vaca Muerta and Picún Leufú Formations): a multi-proxy approach, *Bull. Soc. géol. Fr.* 188: 34.